

**HRP-labeling of bacterial extracellular vesicles for
transmission electron microscopy imaging**

Henna Matero

Master's Thesis
University of Oulu
Degree Programme in Biology
February 2022

Abstract

Extracellular vesicles (EVs) are small, membrane-bound carriers secreted by all cells. In humans, in addition to body's own cells, also the bacteria of the microbiota releases bacterial EVs (BEVs). BEVs in human body can be examined from body fluids. For studying BEVs derived from gut microbiota, fecal samples are used. The isolation protocol of BEVs includes ultrafiltration, size-exclusion chromatography, and density gradient ultracentrifugation. For characterization, transmission electron microscopy and nanoparticle tracking analysis are commonly used. Several methods for labeling and imaging EVs have been demonstrated. Yet, none of them are suitable tracking EVs with high resolution imaging. In this thesis, a novel horseradish peroxidase (HRP) -labeling for BEVs for transmission electron microscopy (TEM) is established. For visualizing the HRP, carrying out a diaminobenzidine (DAB) - reaction had to be optimized. With multiple trials of *in vitro* experiments, a suitable protocol for labeling BEVs was established. As a result of successful HRP-labeling followed by DAB-reaction, BEVs appeared sharply stained on the edges. Further trials in *ex vivo* conditions were performed by injecting HRP-labeled BEVs to a muscle of a euthanized mouse. Thin sections of mouse muscle tissue in TEM revealed dark-stained clusters of structures resembling BEVs. The outcomes of the *ex vivo* mouse experiment were promising but will require optimizing in future studies.

Tiivistelmä

Kaikki solut erittävät ulkopuolelleen kuljetukseen erikoistuneita pieniä kalvopeitteisiä rakkuloita, solunulkoisia vesikkeleitä. Solunulkoisia vesikkeleitä tuottavat paitsi elimistön omat solut, myös elimistössä elävän mikrobiomin solut. Ihmiselimistön suolistobakteerien tuottamia bakteeriperäisiä solunulkoisia vesikkeleitä tutkitaan ulosteesta, joiden eristämiseksi määrittämiseksi ja tutkimiseksi yhdistellään useita eri menetelmiä. Myös vesikkeleiden leimaamiseen ja kuvaamiseen on kehitetty useita menetelmiä, mutta mikään niistä ei sovellu solunulkoisten vesikkeleiden seurantaan läpäisyelektronimikroskoopilla.

Tässä työssä testattiin menetelmää bakteeriperäisten solunulkoisten vesikkeleiden leimaamiseen piparjuuriperoksidaasilla (horseradish peroxidase, HRP). HRP:n havaitsemiseksi menetelmää varten optimoitiin myös diaminobentsidiinireaktio (DAB). Useiden kokeilujen jälkeen sopiva protokolla bakteeriperäisten solunulkoisten vesikkeleiden leimaamiseksi saavutettiin *in vitro* -olosuhteissa. Onnistuneen leimaamisen seurauksena läpäisyelektronimikroskoopissa nähtiin terävästi reunoiltaan värjäytyneitä bakteeriperäisiä solunulkoisia vesikkeleitä. *In vitro* -osuuden jälkeen kokeiluja jatkettiin *ex vivo* -olosuhteissa injektoimalla HRP-leimattuja vesikkeleitä lopetetun hiiren lihakseen.

Läpäisyelektronimikroskoopissa lihaksesta tehdyissä ohutleikenäytteissä nähtiin rykelmiä tummaksi värjäytyneitä, vesikkeleitä muistuttavia rakenteita. Tulokset *ex vivo* -osuudesta olivat lupaavia, mutta vaativat vielä lisätutkimusta tulevaisuudessa.

Table of Contents

List of abbreviations	4
1. Introduction.....	5
1.1. Aims and hypotheses.....	5
2. Literature.....	6
2.1. Extracellular vesicles.....	6
2.1.1. Extracellular vesicle cargo	6
2.1.2. Extracellular vesicle release and binding	8
2.2. Classification of extracellular vesicles	8
2.2.1. Eukaryotic extracellular vesicles.....	9
2.2.2. Bacterial extracellular vesicles.....	10
2.3. Extracellular vesicle functions in health and disease	12
2.4. Isolation and characterization of bacterial extracellular vesicles	13
2.4.1. Isolation	14
2.4.2. Characterization	14
2.4.3. Labeling and imaging	15
3. Materials and methods	18
3.1. Isolation of extracellular vesicles	18
3.1.1. Ultrafiltration and size-exclusion chromatography.....	18
3.1.2. Density gradient ultracentrifugation	19
3.2. Characterization of extracellular vesicles.....	21
3.2.1. Transmission electron microscopy.....	21
3.2.2. Nanoparticle tracking analysis	21
3.2.3. Protein concentration measurement	22
3.3. Labeling bacterial extracellular vesicles	22
3.3.1. HRP-labeling	22
3.3.2. DAB-reaction and sample preparation for imaging	24
3.4. <i>Ex vivo</i> mouse experiment	26
4. Results.....	27
4.1. Isolation and characterization.....	27
4.1.1. Transmission electron microscopy.....	27
4.1.2. Nanoparticle tracking analysis	30
4.1.3. Protein concentration measurements.....	32
4.2. HRP-labeling.....	34
4.3. <i>Ex vivo</i> mouse experiment	38
5. Discussion.....	42
6. Conclusions.....	44
Acknowledgements	45
References	46

List of abbreviations

BEV	bacterial extracellular vesicle
CMV	cytoplasmic membrane vesicle
CT	computer tomography
DAB	diaminobenzidine
EOMV	explosive outer membrane vesicle
ESCRT	endosomal sorting complex required for transport
EV	extracellular vesicle
GNP	gold nanoparticles
HRP	horseradish peroxidase
ILV	intraluminal vesicle
LPS	lipopolysaccharide
MRI	magnetic resonance imaging
MVB	multivesicular body
NTA	nanoparticle tracking analysis
OIMV	outer-inner membrane vesicle
OMV	outer membrane vesicle
PBS	phosphate buffered saline
PET	positron emission tomography
SEC	size-exclusion chromatography
SPECT	single photoemission computed tomography
SPION	superparamagnetic iron oxide nanoparticle
TEM	transmission electron microscopy
TSMS	tube-shaped membranous structure
UA	uranyl acetate

1. Introduction

In human body, not only the body's own cells but also the microbiota of the human body, produces extracellular vesicles (EVs). There are millions of microbes, such as bacteria and archaea in human body, most of them living in the gut, which all can release EVs to their environment.

Due to the great diversity of EVs, the classification is not quite clear yet. There are multiple different names concerning these vesicles according to their origin and nature, such as membrane vesicles, microvesicles, microparticles, exosomes, ectosomes, oncosomes, and apoptotic bodies. Nevertheless, the term "extracellular vesicle" is the most used and therefore also used in this thesis, referring to vesicles from both eukaryotic and bacterial origin.

Various methods for labeling and imaging EVs have been established. However, none of them is suitable for tracking EVs with transmission microscopy imaging (TEM). With the high resolution of TEM imaging, EVs and their functions could be examined on a cellular level.

In this thesis I have examined a novel labeling method of bacterial extracellular vesicles (BEVs) for TEM. Horseradish peroxidase (HRP) -labeling with diaminobenzidine (DAB) -reaction was tested in multiple conditions *in vitro*, and finally in a mouse model, *ex vivo*. Results of the labeling procedure were examined via TEM imaging.

1.1. Aims and hypotheses

The aim of this thesis was to identify the clearest labeling protocol of BEVs for TEM. In addition to *in vitro* testing, the aim was to verify if this labeling protocol is applicable for *ex vivo* mouse model. With a suitable labeling protocol, high resolution imaging of BEVs could be achieved.

The hypothesis was that BEVs would appear stained on the edges in TEM in both *in vitro* and *ex vivo* conditions. Staining on the edges of BEVs would appear since the osmium, used in DAB-reaction, binds to lipid-containing membranes. This way BEVs injected to mouse could be separated from other membrane-covered organelles and particles in tissues.

2. Literature

2.1. Extracellular vesicles

All types of cells, both eukaryotic and prokaryotic, release small membrane-bound carriers to their extracellular environment. These EVs are small, most commonly 20–500 nm in size and can carry varying molecular cargo (Maas et al, 2017; Raposo & Stoorvogel, 2013). They are originated either from endosomes or cell's plasma membrane (Maas et al. 2017). EVs resemble the structure of cells: they are covered with lipid bilayer containing extracellular receptors and ligands and have cytoplasmic proteins and nucleic acids inside. The structure of EVs gives the inner molecules a protected way to be transported between cells and organelles (Maas et al. 2017).

Functions of EVs vary and depend on the interaction and delivery of the cargo to the recipient cell. EVs are a form of intercellular communication which is a vital condition for multicellular organisms (Gurunathan et al. 2019). In addition to their ability of carrying and exchanging compounds between cells, EVs have a role in cells homeostatic signaling and in physiological and pathological states in single- and multicellular organisms (Yáñez-Mó et al. 2015). EVs have also been shown to be involved in elimination of harmful molecules in cells (Maas et al. 2017). With all these properties, their potential in clinical applications, such as biomarkers or drug delivery vehicles seem promising (Mizrak et al. 2013; Pan et al. 2014; Puhka et al. 2017).

EVs produced by human cells have been in a research focus during the past decade. BEVs in human body fluids remain less investigated because of the challenges in separating them from eukaryotic EVs (Tulkens et al. 2020).

2.1.1. Extracellular vesicle cargo

The composition of cargo in EVs generally represents the parental cell (Raposo & Stoorvogel, 2013). Between cells EVs carry and transfer membrane and cytosolic proteins, lipids, carbohydrates, nucleic acids, and small molecular metabolites (Gurunathan et al 2019; Gill et al. 2018; Puhka et al. 2017). Cargo is released by membrane-fusion or endocytosis

with the recipient cell (Gill et al. 2018). Due to the structure of EVs, lipids together with hydrophobic and insoluble proteins can be carried and secreted (Guerrero-Mandujano et al. 2017). EV cargo has been mainly studied with eukaryotic EVs.

Proteins have been found both inside EVs and on their surface, attached to the lipid bilayer, suggesting their roles not only in biogenesis but also in cell-to-cell communication (Maas et al. 2017). EVs are often enriched with endosomal or membrane proteins depending on their origin, as well as proteins associated with lipid rafts (Raposo & Stoorvogel, 2013). Proteins on the surface of EVs, like integrins and tetraspanin complexes, and their interactions with plasma membrane receptors have a major role in target cell specificity (Hoshino et al. 2015; Rana et al. 2012).

Lipids have a role in EV biogenesis in membrane deformation and transport in membrane fission and fusion (Gurunathan et al. 2019). Of lipids, there are usually high amounts of cholesterol, sphingomyelin, and hexocylceramides (Raposo & Stoorvogel, 2013). The stability of EVs as carriers of cellular material is determined by the lipid content of their membranes (Maas et al. 2017).

EVs also carry nucleic acids, such as DNA, mRNA, and a variety of small non-coding RNAs between cells in long-distance transfer (Gill et al. 2018; Raposo & Stoorvogel, 2013). RNA content in EV cargoes has been shown to correlate with the RNA content of the originating cells, but the sorting of RNA species to EVs remains unclear (Raposo & Stoorvogel, 2013). Fusion of DNA-carrying EVs has been thought to be a novel mechanism of horizontal gene transfer in prokaryotes (Gill et al. 2018).

Small molecular metabolites have also been studied in human EVs. A shared metabolic profile of EVs contains for example amino acids, amine metabolites, nucleotides, lipids, and tricarboxylic acid cycle intermediates (Puhka et al. 2017; Zhao et al. 2016). Some metabolites are represented only in specific types of EVs (Puhka et al. 2017). Small molecule metabolites can be originated from inside the cell along cellular pathways or by sorting to EVs from cytosol (Puhka et al. 2017). Since EVs contain metabolic enzymes, small molecule metabolites could also be a product of enzymatic activity inside EVs (Conde-Vancells et al. 2008). The significance of these metabolites remains unclear but is suggested to either act as part of the cargo or be products of their inner enzymatic activity (Puhka et al. 2017; Zhao et al. 2016).

2.1.2. Extracellular vesicle release and binding

In human cells, EVs with their targeted cargoes are formed by budding of the cell membrane and then released by fission. Various cellular systems are associated in EV formation and release: co-operation of the cytoskeleton, molecular motors and switchers together with the fusion machinery are required (Raposo & Stoorvogel, 2013). In bacteria, release of BEVs depends on the subtype of the vesicle.

EV binding prefers acidic conditions and similar lipid composition together with close apposition of the EV and plasma membrane of the recipient cell (Maas et al. 2017). In EVs, binding to the recipient cell is determined by integrins or other adhesion molecules and targeting to recipient cell also requires ligand-receptor binding between EV and the cell (Maas et al. 2017; Raposo & Stoorvogel, 2013). After binding, EVs either associate with the cell membrane, fuse with it, or get endocytosed by the recipient cell (Raposo & Stoorvogel, 2013). If endocytosed to a eukaryotic cell, EVs can fuse with endosomal membrane or get targeted to lysosomes (Maas et al. 2017).

In eukaryotes, EV cargoes awake various responses in recipient cells while the most common fate being their degradation in lysosomes. Degraded proteins and lipids act as a source of metabolites for the recipient cell. (Frühbeis et al. 2013) EVs also have an ability to fuse through the membrane of the endocytic pathway and release their cargo to the cytosol of the recipient cell (Skog et al. 2008). BEV cargoes can be transported to eukaryotic cells or other bacterial cells (Bitto et al. 2017).

2.2. Classification of extracellular vesicles

EVs are highly heterogeneous. In eukaryotes they can be classified to exosomes, microvesicles and apoptotic bodies based on their size and the mechanism of their release (Gurunathan et al. 2019). In bacteria the classification is based on the membrane the vesicles are originated from (Gill et al. 2018).

2.2.1. Eukaryotic extracellular vesicles

Exosomes are 30-150 nm in diameter sized membrane vesicles that are released from cells multivesicular bodies (MVBs) via exocytosis. Exosomal cargo varies and depends on the metabolic state of the cell of origin (Gurunathan et al. 2019). Biogenesis of exosomes begins with invagination of the cell membrane forming endosomes inside the parental cell. This in-budding of the membrane causes the formation of MVBs containing intra-luminal vesicles (ILVs) (Gurunathan et al. 2019). The best-known mechanism for exosome biogenesis involves endosomal sorting complex required for transport (ESCRT) machinery, which transports ubiquitinated cargoes to early endosomes and form ILVs and finally MVBs (Maas et al. 2017). Other known mechanisms of exosome biogenesis involve ceramide synthesis or tetraspanin-mediation of specific protein organization (Maas et al. 2017). After transportation and correct apposition, MVB fusion with the cell membrane causes release of the ILVs as exosomes to the extracellular environment via exocytosis (Gurunathan et al. 2019). Alternatively, exosomes can be released to lysosomes causing recycling of the EV content (Maas et al. 2017).

Microvesicles, usually 200-500 nm in diameter, shed from the plasma membrane of various cell types by outward-budding and fission (Maas et al. 2017). Since they have been shown to occur especially in tumor cells, the shedding of microvesicles has been associated with tumor invasion and formation of metastases (Muralidharan-Chari et al. 2010). Smaller EVs, under 100 nm in diameter have also been found to shed similarly, as well as much bigger EVs called large oncosomes, ranging from 1 to 10 μm in diameter (Maas et al. 2017). The mechanism of biogenesis for microvesicles remains poorly understood but has been thought to involve the same ESCRT machinery like in exosomes. EV budding can also respond to wounding of the plasma membrane of the cell. In addition, asymmetry of the plasma membrane causing activation of the lipid-transferring enzymes has been shown to promote vesicle budding (Maas et al. 2017). In the biogenesis of microvesicles, several changes in molecular components, such as in lipid and protein composition, are needed for the plasma membrane to bend and bud. Regulation of the cytoskeletal elements are also required (Piccin et al. 2007). The release of microvesicles has been suggested to happen similarly as in abscission in the cytokinesis or as viral budding, where the membrane connection of the two cells is abruptly (Muralidharan-Chari et al. 2010).

Apoptotic bodies are formed during apoptosis where a cell is decomposed into vesicles of different sizes. The amount of genomic DNA is thought to be higher in apoptotic bodies than in other subtypes of EVs because of the nature of their biogenesis (Maas et al. 2017).

2.2.2. Bacterial extracellular vesicles

Bacteria produce EVs with sizes from 20 to 400 nm in diameter. Their various roles in biological processes include cell-to-cell communication and transport of cellular metabolites, virulence and phage infection, and horizontal gene transfer (Toyofuku et al. 2019). In the human body, BEVs are enriched in organized structures of microbes referred to as biofilms and their production has been shown to increase also during infections (Gill et al. 2018).

Multiple models of BEV biogenesis have been proposed but the mechanisms are still not fully understood (Gill et al. 2018). BEVs form both from living cells and during cell lysis (Toyofuku et al. 2019). BEV distribution to subtypes depends both on the bacterial species and its state of physiology (Tulkens et al. 2020).

Characterization of bacteria, as well as EVs they produce, is based on the thickness of peptidoglycan in their cell wall (Gill et al. 2018). Most of the bacteria are gram-negative, meaning they have an outer membrane of lipopolysaccharide (LPS) over a thin layer of peptidoglycan in their periplasmic space. Gram-positive bacteria have only a thick layer of peptidoglycan, without an outer membrane (Gill et al. 2018).

2.2.2.1. Outer membrane vesicles

Outer membrane vesicles, or OMVs, are produced by gram-negative bacteria by blebbing of the outer membrane (Gill et al. 2018). OMVs have an outer leaflet of LPS and inner leaflet of phospholipid (Toyofuku et al. 2019). Because of the two membranes of the bacteria of origin, OMVs are usually enriched in periplasmic cell components, such as lipids, membrane proteins, lipoproteins, and glycolipids (Gill et al. 2018). Cytosolic cell components, such as DNA and RNA, have also been found in OMVs, but the sorting mechanism remains unknown (Toyofuku et al. 2019).

Several mechanisms for OMV blebbing have been proposed. Unsuccessful crosslinking of peptidoglycan and the outer membrane causes disturbances in the cell envelope leading to blebbing of the membrane and OMV formation (Toyofuku et al. 2019). Behind vesiculation, multiple genes encoding mainly the components of the bacterial envelope are examined. Environmental factors act both directly on vesicle formation and by affecting the expression of these genes (Toyofuku et al. 2019).

OMVs act as a specialized secretion pathway in bacteria (Toyofuku et al. 2019). In addition to intercellular communication, they have been linked to stress response, formation of biofilms, antibiotic resistance, and delivery of toxins. (Gill et al. 2018) In bacterial colonization, OMVs can regulate the growth of other microbial cells by secreting enzymes and antibiotics to their environment (Toyofuku et al. 2019). Cargo transport to eukaryotic cells is also possible via OMVs and has been shown to emerge in pathogenesis and in the regulation of homeostasis (Gill et al. 2018).

2.2.2.2. Outer-inner membrane vesicles

Outer-inner membrane vesicles, or OIMVs, are produced by diverse bacteria originating from the inner, cytoplasmic membrane (Gill et al. 2018; Toyofuku et al. 2019). They contain both periplasmic and cytoplasmic cell components, including DNA, RNA and ATP (Gill et al. 2018).

According to Toyofuku et al. (2019), in OIMVs, the peptidoglycan cell wall is partially degraded by peptidoglycan hydrolases called autolysins. Due to this degradation, also cytosolic components can be sorted to vesicles. Another explanation for cytosolic components in MVs is explosive cell lysis, where bacteriophages degrade the cell wall of the host cell causing exploding of the cell. In addition to OIMVs, formation of OMVs and cytoplasmic membrane vesicles (CMVs) via this route is possible but still unclear. OMVs formed from explosive cell lysis are referred to as explosive outer membrane vesicles (EOMVs).

2.2.2.3. Cytoplasmic membrane vesicles

Gram-positive bacteria have been shown to produce EVs despite the thick cell wall. These BEVs are often referred as cytoplasmic membrane vesicles or CMVs. They have been found to originate from dying cells but considered to rise from living cells as well (Toyofuku et al. 2019). CMVs seem to produce enzymes that locally destruct the layer of peptidoglycan and allow vesicles to cross the barrier. (Gill et al. 2018)

Gram-positive bacteria dissociate by pushing cytoplasmic material through holes in the cell wall, forming CMVs. (Toyofuku et al. 2019) The event is similar to explosive cell lysis, although termed bubbling cell death. Both membrane and cytoplasmic components have been found inside CMVs. (Toyofuku et al. 2019)

2.2.2.4. Tube-shaped membranous structures

As stated in Toyofuku et al. (2019), specialized types of membrane vesicles, called nanotubes, nanopods or nanowires, originate from diverse bacteria, including both gram-negative and gram-positive ones. These tube-shaped membranous structures, commonly called TSMSs, are found on the surface of cells or on bridges formed between two cells. The size of TSMSs vary from 30 to 60 nm in width and up to 5 μm in length. TSMSs form a membrane-enclosed connection between periplasmic spaces of two cells allowing them to exchange components. OMVs seem to be able of getting organized as strings forming nanotubes and, in turn, nanotubes are observed to have the ability to break down to OMVs. The formation of TSMSs is assumed to require local lysis of the cell wall and an outward bulge of the membrane.

2.3. Extracellular vesicle functions in health and disease

EVs are involved in various biological processes due to their ability to transfer compounds between cells both locally and at distance. They have a role in recycling molecules and removing excess cellular components from cells. EVs also affect processes behind various infections and diseases (Raposo & Stoorvogel, 2013). EVs have been shown to play a role in inflammatory conditions (van Niel et al. 2001). They have also been associated with tumor

progression (Kim et al. 2002) and suppression of immune responses (Zhang & Grizzle, 2011) as well as pathogenic proteins, like prions, in central nervous system (Fevrier et al. 2004). Pathogenic bacteria have been shown to use EVs as delivery vehicles for toxic compounds (Bitto et al. 2017). In addition to affecting other cells, EVs are also able of provoking autocrine responses by targeting to the cell membrane receptors of the producing cell itself (Matsumoto et al. 2017).

EVs have many common features with virions and the interactions between them have been researched (Martins & Alvens, 2020). Viruses can use EVs of infected cells for their multiplication purposes (Altan-Bonnet & Chen, 2015). However, EVs have also been shown to inhibit the propagation of viruses by transferring antiviral substances (Yao et al. 2018).

BEVs in general have many qualities that promote their use in clinical approaches, like their uptake by mammalian cells. As reported by Jones et al. (2020), it has been shown that BEVs have an ability to cross intestinal epithelial cell barrier by paracellularly passing through intercellular space of epithelial cells. This indicates that BEVs from the microbiota of the gastrointestinal tract can migrate to blood circulation and lymphatic system of the body, eventually entering systemic organs. In addition to crossing intestinal epithelial barrier, BEVs have been demonstrated to also cross the blood-brain barrier allowing them to enter the brain (Wei et al. 2020).

EV related research aims for clinical approaches, such as using EVs as biomarkers for disease, drug delivery devices or for vaccines (Raposo & Stoorvogel, 2013). For example, EVs are considered as potential biomarkers for cancer diagnostics (Puhka et al. 2017), and exosomes from hepatocytes were seen to carry proteins that could act as biomarkers for diseases (Conde-Vancells et al. 2008). OMVs have already been used in vaccine development (Nøkleby et al. 2007).

2.4. Isolation and characterization of bacterial extracellular vesicles

EVs have been isolated from various types of body fluids such as blood, semen, bile, saliva, feces, breast milk, and amniotic fluid (Raposo & Stoorvogel, 2013). For isolating EVs from biological samples, multiple methods are combined. Ultrafiltration is often used together with size-exclusion chromatography (SEC) and density gradient ultracentrifugation (Gurunathan et al. 2019). Ultrafiltration together with SEC separates BEVs from cell debris, bacteria, and

flagella and following density gradient ultracentrifugation separates lipoproteins, fibers, protein aggregates, and eukaryotic EVs (Tulkens et al. 2020). In feces, which is the sample type used in this thesis, BEVs overlap with eukaryotic EVs and protein aggregates in size, and with pili and flagella in density (Tulkens et al. 2020).

2.4.1. Isolation

Ultrafiltration and SEC are often used together for obtaining good quality yields of isolated EVs. In ultrafiltration, EVs are isolated by their size or molecular weight using membrane filters, where defined filter pore size leads to removal of unwanted material in the sample (Benedikter et al. 2017; Gurunathan et al. 2019). In EV isolation, 10 kDa filters have been shown to result in complete recovery of the vesicles (Benedikter et al. 2017). In SEC, particles are separated based on their molecular size. Samples are centrifuged through pores in chromatography column matrix with an eluent. Small particles are included in the pores whereas large particles pass the column faster and eluate first (Tulkens et al. 2020) As a result, the formed eluate contains EVs while other particles are delayed (Benedikter et al. 2017).

Density gradient ultracentrifugation is a method used for isolating and fractioning EVs and other biological components in samples (Gurunathan et al. 2019). With high centrifugal forces, EV subtypes can be separated (Van Deun et al. 2014). Combination of ultrafiltration and SEC result in a sample with high yield but low specificity of BEVs, whereas density gradient ultracentrifugation returns a sample of low yield but high specificity in the fractions identified to hold the BEVs (Tulkens et al. 2020). In contrast to other methods, use of OptiPrep® density gradient ultracentrifugation for BEV isolation has been shown to result in the purest yield (Van Deun et al. 2014).

2.4.2. Characterization

Various techniques are used for further characterization of isolated EVs, including transmission electron microscopy and nanoparticle tracking analysis.

Transmission electron microscopy is a commonly used imaging technique to visualize isolated EVs. In TEM, a beam of electrons passes through a sample generating secondary

electrons that are collected and magnified, which then creates the images (Gurunathan et al. 2019). Samples are fixed with glutaraldehyde, dehydrated on a grid, and then imaged under vacuum condition (Gurunathan et al. 2019). With TEM, both single and double bilayered BEVs can be identified (Tulkens et al. 2020). Purity of the sample can be estimated by the amount of viral-, flagellar or pilin constructs present. These filamentous structures can be enriched in the sample fractions holding the BEVs (Langlete et al. 2019).

Nanoparticle tracking analysis (NTA) is a biophysical method for evaluating the properties of individual nanosized particles as well as their quantification (Gurunathan et al. 2019) It is an optical particle tracking approach which detects the movement of nanoparticles, called Brownian motion, in a liquid suspension. NTA tracks each particle via image analysis and correlates the particle movement to particle size giving the output of individual particle size, size distribution and concentration. (Gurunathan et al. 2019) NTA is commonly used together with imaging methods. (Tulkens et al. 2020)

In addition to TEM and NTA, the amount of protein in samples can be measured for estimating the EV concentration. Absorbance measurements and colorimetric assays can be performed via spectrophotometric protein assays. In absorbance measurements, purified proteins containing certain bonds (280 nm absorbance) can be quantified fast whereas in colorimetric assays, preparation of a standard curve is required for measuring uncharacterized protein solutions together with cell lysates (Thermo Fisher Scientific, 2016).

2.4.3. Labeling and imaging

EVs can be visualized and tracked with different techniques which include fluorescence imaging, bioluminescence imaging, nuclear imaging, and tomography imaging.

In fluorescence imaging, EVs are fluorescently labeled using fluorophores. Fluorescently labeled EVs emit fluorescent signals and can be detected with fluorescent microscopy or qualitative fluorometry. Commercial membrane dyes, like PKH, DiI and DiR, are commonly used. They are lipophilic and bind to the bilayer of the vesicles (Choi & Lee, 2016). Besides membrane dyes, aggregation induced emission luminogens have been used for labeling EVs with some limitations (Cao et al. 2019). In addition, fluorescent protein reporters (Wiklander

et al. 2015) and other chemicals containing fluorophores, e.g., chemotherapeutic drugs (Ingato et al. 2018), have been used.

Bioluminescence imaging is a method where light emission from luciferase enzyme-substrate reaction is detected with a special camera. Luciferase enzymes are found and isolated from living organisms for biomedical purposes (Badr & Tannous, 2011). For example, Gaussia luciferase enzyme has successfully been joined with a transmembrane domain for creating fusion proteins to label vesicles and identifying their location in tissues (Takahashi et al. 2013). Other luciferase enzymes, such as Firefly luciferase (Kanada et al. 2015) and Renilla luciferase (Gangadaran et al. 2017), have also been used in bioluminescence labeling of EVs.

Nuclear imaging, including single photoemission computed tomography (SPECT) and positron emission tomography (PET) is a widely used noninvasive imaging method. In nuclear imaging, EVs are labeled with radioisotopes which emit gamma or positron radionuclides that can be detected with special instruments (Almeida et al. 2020). In previous studies, different radioisotopes have been tested for labeling EVs. For example, 125-Iodine labeled EVs (Morishita et al. 2015) and 111-Indium-oxine labeled EVs (Smyth et al. 2015) have been traced in mice by following the radioactivity levels in blood *in vivo* and in organs *ex vivo*.

Tomography imaging is a noninvasive method which requires computer tomography (CT) or magnetic resonance imaging (MRI) equipment. For tomography imaging, EVs need to be labeled with nanoparticles by electroporation (Busato et al. 2016). Commonly used nanoparticles include gold nanoparticles (GNPs) and superparamagnetic iron oxide nanoparticles (SPIONs). For example, glucose-coated GNPs have successfully been used for noninvasive tracking of EVs in mice with CT (Betzer et al. 2017). SPION-labeled EVs have been tracked both *in vitro* and *in vivo* via MRI in mice (Hu et al. 2015).

EV labeling methods for TEM imaging have not been established. In TEM, the visualization of biological structures is obtained by creating contrast between the structures and embedding media with heavy metals, such as osmium (Ellis, 2014). Uranyl acetate (UA) is another widely used reagent for creating contrast in TEM-stains (Brenner & Horne, 1959). In addition to reagents, thickness of the section with accelerating voltage and the size of aperture of the microscope also have an impact on the contrast of the sample (Ellis, 2014). For stabilizing the biological structures in the samples, glutaraldehyde is commonly used as a fixative (Hayat, 1986).

With suitable labeling, TEM could offer higher resolution imaging of EVs than previous methods (Yong-Jiang et al. 2020). One potential option for labeling EVs includes HRP together with DAB-reaction. HRP is a widely studied enzyme label which activity can be detected and visualized via chromogenic substrates, like DAB (Azevedo et al. 2003; Rodig, 2019). With the presence of nitrogen peroxide, HRP and DAB can form a product that can be detected with electron microscopy (Azevedo et al. 2003).

3. Materials and methods

3.1. Isolation of extracellular vesicles

In this thesis, BEVs were isolated from five human fecal samples and six mouse fecal samples, using a protocol provided by Group Reunanen, according to Tulkens et al. 2020. Human fecal samples from healthy individuals were collected and frozen earlier at -80°C . Mouse fecal samples were collected directly from mice ceca in Laboratory Animal Center in University of Oulu. Used mice were from strain C57BL/6, which is a commonly used inbred strain of laboratory mice. Altogether seven mice (H1– H7) were killed using carbon dioxide followed by heart perfusion performed with heparinized PBS at 10 ml/min speed. In addition to feces, a set of mice organs were also harvested, weighted and frozen immediately to liquid nitrogen. Mice organs were left unused in terms of this thesis but stored at -80°C for further use in the lab to reduce the amount of the mice needed for experiments.

All fecal samples were kept at -80°C and thawed on ice before proceeding. The amount of used sample differed, human fecal matter being around 600 mg (568–618 mg) and mouse fecal matter varying between 24 mg and 484 mg, depending on the amount collected from the cecum of individual mouse. Isolation was performed in five separate rounds to ensure good quality of the procedure. Altogether four rounds of human fecal vesicles and one rounds of mouse fecal vesicles were isolated.

3.1.1. Ultrafiltration and size-exclusion chromatography

Fecal samples were suspended to cold, sterile-filtered phosphate buffered saline (PBS) in Falcon tubes by pipetting the solution back and forth and then centrifuged at 14 000 g for 30 min at $+4^{\circ}\text{C}$ for pelleting the debris. Supernatants were centrifuged again and filtered twice, first using 40 μm nylon filter (Falcon® Cell Strainer, Corning) and then using 0.45 μm PES-filter (Vacuum Bottle Filter, Biofil) to remove cells and rest of the cell debris.

On the next step, samples were concentrated by ultrafiltration using 10 kDa centrifugal filter units (Amicon® Ultra-15, Millipore). Samples were centrifuged with a swinging bucket rotor at 3000 g for 30 min at $+4^{\circ}\text{C}$ and then collected from the filter unit. After concentration the volume of each sample was reduced from 12 ml to approximately 200 μl . Some samples were

concentrated twice if the volume of the concentrate was remarkably higher than expected. For isolating the vesicles, commercial size-exclusion chromatography (SEC) columns (Exo-Spin™ Mini-Columns, Cell Guidance Systems) were used according to user guide (provided in Exo-Spin™ Exosome Purification Kit). The yield of the eluate obtained was about 200 µl per sample.

3.1.2. Density gradient ultracentrifugation

Iodixanol density gradient centrifugation was used for purification of the samples as a variation of OptiPrep® density gradient centrifugation protocol by Van Deun et al. (2014). Homogenation buffer and working solution buffer were prepared for gradient solutions. (Table 1). Gradient solutions (5 %, 10 %, 20 % and 40 % concentrations) were prepared with homogenation buffer and working solution (Table 2). For working solution, iodixanol (OptiPrep®, Fisher Scientific) gradient media and working solution buffer were used.

Table 1. Preparation of homogenation buffer and working solution buffer for density gradient ultracentrifugation

Homogenation buffer (pH 7.4)			
Reagent	Final concentration	Weight	Volume
Sucrose	1M	-	125 ml
Tris-HCl	1M	-	5 ml
EDTA	1 mM	0.1861 g	-
Total volume 500 ml (filled up with sterile H ₂ O after adjusting pH). Filtered with 0.45 µm filter unit before use.			
Working solution buffer (pH 7.4)			
Reagent	Final concentration	Weight	Volume
Sucrose	0.25 M	-	125 ml
Tris-HCl	60 mM	-	30 ml
EDTA	6 mM	1.1166 g	-
Total volume 500 ml (filled up with sterile H ₂ O after adjusting pH). Filtered with 0.45 µm filter unit before use.			

Table 2. Pipetting instructions for gradient solutions for density gradient ultracentrifugation (for 6 samples)

Percentage	Working solution (4.5 ml working solution buffer + 22.5 ml OptiPrep® gradient media)	Homogenation buffer
5	1.5 ml	13.5 ml
10	3.4 ml	13.6 ml
20	6.8 ml	10.2 ml
40	3.6 ml	3.4 ml

Top-down gradients were prepared by carefully pipetting 2.5 ml of 40 %, 20 %, and 10 % solutions on top of each other, followed by 2.2 ml of 5 % solution on top of the tube. 200 μ l of the concentrated samples were then pipetted on top of the gradients and centrifuged in ultracentrifuge (Beckmann Optima L-100/L-90) with a swinging bucket rotor (SW 41 Ti) at 100 000 g for 18 hours at +4 °C.

After overnight ultracentrifugation, fractions were pipetted 1 ml at a time, one fraction per Eppendorf tube. Pipetting was done by hand, carefully from the gradient surface avoiding mixing between the fractions. Fractions 6 and 7, presumably holding the EVs from bacterial origin, were transferred to 15 ml Falcon tubes and then washed with PBS via ultracentrifugation at 100 000 g for 3 hours at +4 °C. Supernatants were discarded by pouring, and the remaining pellet (typically invisible) was resuspended to 100 μ l of PBS. Aliquots for TEM (7 μ l), NTA (20 μ l), and protein measurements (5 μ l) were taken, and rest of the sample was frozen to -20 °C.

3.2. Characterization of extracellular vesicles

Success of the isolation of was confirmed with both TEM and NTA. Both measurements were performed individually for each sample.

3.2.1. Transmission electron microscopy

For TEM imaging of the samples, Tecnai G2 Spirit with 18 500–49 000 x magnification was used. Negative staining of samples was performed by the EM Core facility service of the University of Oulu by the established protocol. From each grid, samples were imaged from five spots for getting an overall look of the whole grid.

In TEM, BEVs were characterized by their visual appearance. Most characteristic feature of vesicles in general is the bilayer membrane, which can often be seen in TEM. Also, their known size (varying from 20 to 500 nm) and their round, cup-shaped morphology are some features to look for. In addition to BEVs, some filamentous structures left from the purification steps, might be seen.

3.2.2. Nanoparticle tracking analysis

NTA was performed with NanoSight NS300 instrument using NTA software v3.3.104 according to the manufacturer's guidelines. The system was washed multiple times by injecting sterile water to sample injection tube. Washing was done before and in between the measurements until the image seemed clear of particles. Image was then focused with the focus wheel and by adjusting the screen. Samples were loaded to the system one at a time with a syringe pump which automatically inserted the sample inside the system according to the program script. Screen gain was set to 7 and camera level to 14. Detection threshold was adjusted after the run and varied between 3 and 5 between samples.

Samples were diluted with sterile PBS in either 1:25 or 1:50 dilution depending on the output concentration on the first detection. Acceptable threshold values for reliable raw data ranged from 5×10^7 to 9×10^8 particles/ml (according to manufacturer's recommendations) and the actual concentrations were calculated multiplying the obtained value with the dilution factor.

3.2.3. Protein concentration measurement

Protein concentrations of the samples were determined to verify the NTA measurement. Two parallel spectrophotometric methods Protein A280 and Pierce™ BCA, were used. Both assays were performed using the same Thermo Fisher Scientific™ Nanodrop 2000 spectrophotometer.

In Protein A280 assay, samples were measured individually. 2 µl of sample was pipetted to the sample pedestal and measured while closing the sampling arm using A280 instrument mode. Instrument was washed with sterile water and wiped with fine paper between the measurements and before the first measurement. PBS was used as a blank.

Pierce™ BCA measurement was performed according to Pierce™ BCA Protein Assay Kit instructions. Standards of known concentrations were prepared right before the measurements using sterile water and 2 mg/ml BCA solution provided in the kit. Samples were measured according to standard curve in a range from 31.25 µg/ml to 1000 µg/ml using Pierce™ BCA mode of the instrument. For three samples out of the range, a higher standard curve was prepared (1000-2000 µg/ml). Three parallel measurements were performed for all standards and samples. Otherwise, the instrument was used similarly as in Protein A280 method.

3.3. Labeling bacterial extracellular vesicles

BEVs are labeled for tracking them inside the tissues *ex vivo* after being injected into mouse. In scope of this thesis, HRP labeling followed by DAB-reaction was used. Only BEVs isolated from human feces were used for labeling. BEVs from mouse feces were frozen at -20 °C for further use.

3.3.1. HRP-labeling

In HRP-labeling, vesicles are labeled with HRP and visualized with DAB-reaction. Labeling was repeated four independent times *in vitro* before the mouse experiment. For these trials, BEVs from a mixture of six human fecal samples of fourth isolation round were used.

Traut's reagent (G-Biosciences®) was first used for pre-treatment of HRP as gentle thiolation agent according to manufacturer's recommendations. In thiolation, free sulfhydryl groups are introduced to protein, here to HRP for crosslinking. 3 mg of HRP (10 mg/ml stock) was incubated with 2-fold molar excess (9.358 μ l) of Traut's reagent for 1 hour at room temperature.

Maleimide reaction is needed for chemical conjugation of BEVs (see Figure 1). In this thesis, 4 % maleimide crosslinker (DSPE-PEG, Sigma-Aldrich®) was used to conjugate BEVs with thiolated HRP, which corresponds to 1:530 000 dilution factor of maleimide.

Maleimide stock solution (10 mg/ml) was diluted in 1:530 000 ratio in three steps, first diluting in 1:530 and further to 1:100 ratio with ethanol. The final dilution was done by adding 10 μ l of 1:53 000 diluted maleimide solution to 100 μ l of BEVs, resulting in 1:530 000 dilution. In the first two trials, 5 % maleimide was used instead (corresponding to 1:420 000 dilution factor), which was then changed to 4 % in the last two trials to increase the specificity of crosslinking.

Finally, maleimide-incorporated BEVs were crosslinked to thiolated HRP in 1:1 ratio and incubated at room temperature in a vortex stirrer for 30 minutes before continuing to DAB-reaction.

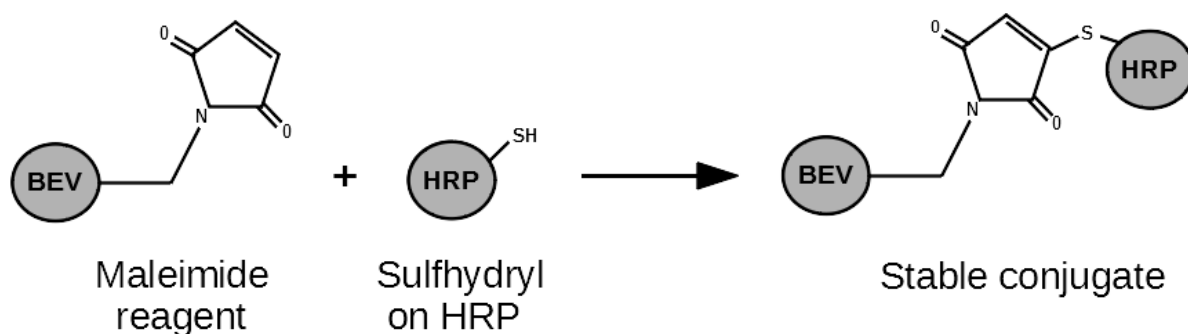


Figure 1. Reaction scheme for conjugation of BEV-incorporated maleimide reagent to sulfhydryl group on thiolated HRP

3.3.2. DAB-reaction and sample preparation for imaging

DAB-reaction was done to HRP-labeled BEVs on grids in four trials. Different incubation times and temperatures of 1 % osmium and 1.5 % potassium ferrocyanide were tested together with UA-coating and glutaraldehyde fixation to optimize the conditions for best visualization in TEM.

For 0.05 % DAB-solution, a DAB-pellet (10 mg, Sigma-Aldrich®) was first diluted into 20 ml of sterile PBS, which was then divided into two 10 ml aliquots. After washing the samples 3 x 5 minutes in cold PBS, they were incubated in DAB-solution for 20 minutes at room temperature, covered from light. Next, samples were incubated in DAB-hydrogen peroxide – solution (10 ml DAB solution + 16 µl H₂O₂) for 30 minutes at room temperature and washed after 3 x 5 minutes in cold PBS. Finally, samples were incubated in TEM-fixative for 30 minutes at +4 °C and washed 3 x 5 minutes in PBS. Final steps of the labeling were carried partially by the EM Core facility service in University of Oulu.

There were 21 different samples tested in four independent trials of HRP-labeling with 14 different conditions altogether. Finally, there were six different tested conditions and eight different negative control conditions. DAB-reaction was done to 19 samples. Two negative controls were done without DAB-reaction (conditions 9 and 10) and were instead negatively stained in the EM Core laboratory. Some conditions were tested twice if the outcome of the first test was unclear and therefore needed to be verified. 1 % osmium and 1.5 % ferrocyanide incubation was performed to all samples, either for 60 minutes at + 4 °C or 30 minutes at room temperature.

Trial 1

Four different conditions were tested in trial 1. Glutaraldehyde was used as fixative in conditions 1 and 2 but left unused in conditions 3 and 4. Uranyl acetate (UA) coating was used for all samples (incubation time 20 min). RT = room temperature

- 1) glutaraldehyde fixed HRP-labeled BEVs, UA, osmium 60 min + 4 °C
- 2) glutaraldehyde fixed HRP-labeled BEVs, UA, osmium 30 min RT
- 3) non-fixed HRP-labeled BEVs, UA, osmium 60 min + 4 °C
- 4) non-fixed HRP-labeled BEVs, UA, osmium 30 min RT

Trial 2

Four new conditions (5–8) together with two negative control samples (8 and 9) were tested in trial 2. Glutaraldehyde was used in all samples without UA-coating.

- 5) glutaraldehyde fixed HRP-labeled BEVs, without UA, osmium 60 min + 4 °C
- 6) glutaraldehyde fixed HRP-labeled BEVs, without UA, osmium 30 min RT
- 7) glutaraldehyde fixed PBS with HRP, without UA, osmium 30 min RT
(negative control)
- 8) glutaraldehyde fixed BEVs with PBS, without UA, osmium 30 min RT
(negative control)
- 9) plain EVs, no HRP-labeling or DAB-reaction (negative control)
- 10) HRP-labeled BEVs, no DAB-reaction (negative control)

Trial 3

In trial 3, UA-coating was used to all samples (incubation time 20 min). Conditions 1–4 were tested already in the first trial but repeated now again together with three novel negative control conditions (11–13).

- 1) glutaraldehyde fixed HRP-labeled BEVs, UA, osmium 60 min +4 °C
- 2) glutaraldehyde fixed HRP-labeled BEVs, UA, osmium 30 min RT
- 3) non-fixed HRP-labeled BEVs, UA, osmium 60 min +4 °C
- 4) non-fixed HRP-labeled BEVs, UA, osmium 30 min RT
- 11) non-fixed PBS with HRP, UA, osmium 30 min RT (negative control)
- 12) non-fixed BEVs with PBS, UA, osmium 30 min RT (negative control)
- 13) only DAB, UA, osmium 30min RT (negative control)

Trial 4

In trial 4, UA-coating was used to all samples (incubation time 20 min). Conditions 2 and 4 together with negative control condition 11 were tested earlier in previous trials and repeated in this trial. Negative control 14 was a novel condition.

- 2) glutaraldehyde fixed HRP-labeled BEVs, UA, osmium 30 min RT
- 4) non-fixed HRP-labeled BEVs, UA, osmium 30 min RT
- 11) non-fixed PBS with HRP, UA, osmium 30 min RT (negative control)
- 14) glutaraldehyde fixed PBS with HRP, UA, osmium 30 min RT (negative control)

3.4. *Ex vivo* mouse experiment

Two muscle injections were performed for one C57BL/N -mouse, which was first killed with carbon dioxide followed by cervical dislocation. Legs of the mouse were skinned before injections for revealing the muscles. Evans Blue dye (Sigma-Aldrich®) was added to sample solutions before injections. It was used to visualize the areas with BEVs after injections.

Injections were performed in Laboratory Animal Center of the University of Oulu. Amount of BEV-solution in injections varied between 50–100 µl. Altogether six muscle samples were taken, two for each condition:

- 1) HRP-labeled BEVs, pre-mixed with Evans Blue
- 2) HRP-labeled BEVs, pre-mixed with Evans Blue
- 3) maleimide-incorporated BEVs without HRP, pre-mixed with Evans Blue
- 4) maleimide-incorporated BEVs without HRP and DAB, pre-mixed with Evans Blue
- 5) plain muscle, no BEVs or Evans Blue (negative control)
- 6) plain muscle, no BEVs or Evans Blue (negative control)

Cutting of the tissue was done under stereomicroscope. All samples, about 2 mm x 2 mm in size, were fixed immediately after cutting in TEM-fixative (1 % glutaraldehyde, 4 % formaldehyde in 0.1 M phosphate buffer) for 90–120 minutes. After fixation, DAB-reaction (with the same protocol as performed for grids) was performed for five tissue samples (conditions 1-3, 5, 6).

After DAB-reaction, samples were placed back to TEM-fixative and taken to EM Core laboratory for plastic embedding and thin sectioning. Another of the two maleimide-BEV-samples (condition 4) acted as a negative control and was kept in the TEM-fixative without DAB-reaction and taken to EM Core laboratory together with other samples. For tissue thin sections, slight differences were made to the tested protocol due to changes in sample material. 1 % osmium + 1.5 % potassium ferrocyanide incubation was done for 2 hours at +4 °C and uranyl acetate was not used for coating. Finally, thin sections were stained with lead citrate for 5 minutes. Results of the labeling were examined via TEM after two weeks.

4. Results

4.1. Isolation and characterization

BEVs were isolated from five healthy individuals (C2, C4, C6, C9 and C12) in four independent rounds. Isolated BEVs were characterized by their morphological appearance (Table 3, Figures 2–3), concentration of individual particles (Table 4, Figure 4) and by amount of protein (Table 5). Since all these methods have some limitations, only characterization via different methods can give the big picture.

The amount of BEVs between the isolation rounds differ in all methods, because the samples are randomly taken from the stocks and many steps of the protocol is done by hand. Also, feces of different individuals inherently contain different amounts of BEVs.

4.1.1. Transmission electron microscopy

From each sample, fractions 6 and 7 (pooled) were checked in TEM for ensuring the success of the isolation (Table 3). In the first rounds, concentration of the BEVs was very low, but the samples were pure, meaning they did not have much excess material, like viral-, flagellar-, or pilin constructs, which are often enriched in the same fractions as BEVs. In further rounds, some small modifications were made to the protocol, including vortexing and mixing the samples more frequently, resulting in better yield of BEVs in following isolations. Following this protocol, the amount of BEVs in samples was moderate. The amount of debris in the fractions was proportional to BEV concentrations. All in all, the isolated fractions were pure and BEVs were successfully characterized according to their size and structure (Figures 2 and 3).

Table 3. Results from fraction quality check in TEM after EV isolations

Round	Sample	Concentration of vesicles, pureness of the fraction
1	C2.1	concentration of vesicles very low, a few flagellas
	C4.1	concentration of vesicles very low, a few virus-like particles
	C6.1	concentration of vesicles very low, pure
	C9.1	concentration of vesicles very low, a few fibrios
2	C2.2	concentration of the vesicles low/moderate, some fibrios
	C4.2	concentration of the vesicles low/moderate, some fibrios
	C6.2	concentration of vesicles very low, pure
	C9.2	concentration of vesicles low, some fibrios
	C12.2	concentration of vesicles moderate, some flagellas
	mix 2 (all)	-
3	C2.3	concentration of vesicles low, some fibrios/flagellas
	C4.3	concentration of vesicles moderate, some fibrios/flagellas
	C6.3	concentration of vesicles very low, pure
	C9.3	concentration of vesicles moderate, some fibrios/flagellas
	C12.3	concentration of vesicles moderate, some fibrios/flagellas
	mix 3 (all)	-
4	C2.4	concentration of vesicles low, some fibrios/flagellas
	C4.4	concentration of vesicles moderate, pure
	C6.4	concentration of vesicles very low, pure
	C9.4	concentration of vesicles moderate, a few fibrios/flagellas
	C12.4	concentration of vesicles moderate, some fibrios/flagellas
	mix 4 (all)	-

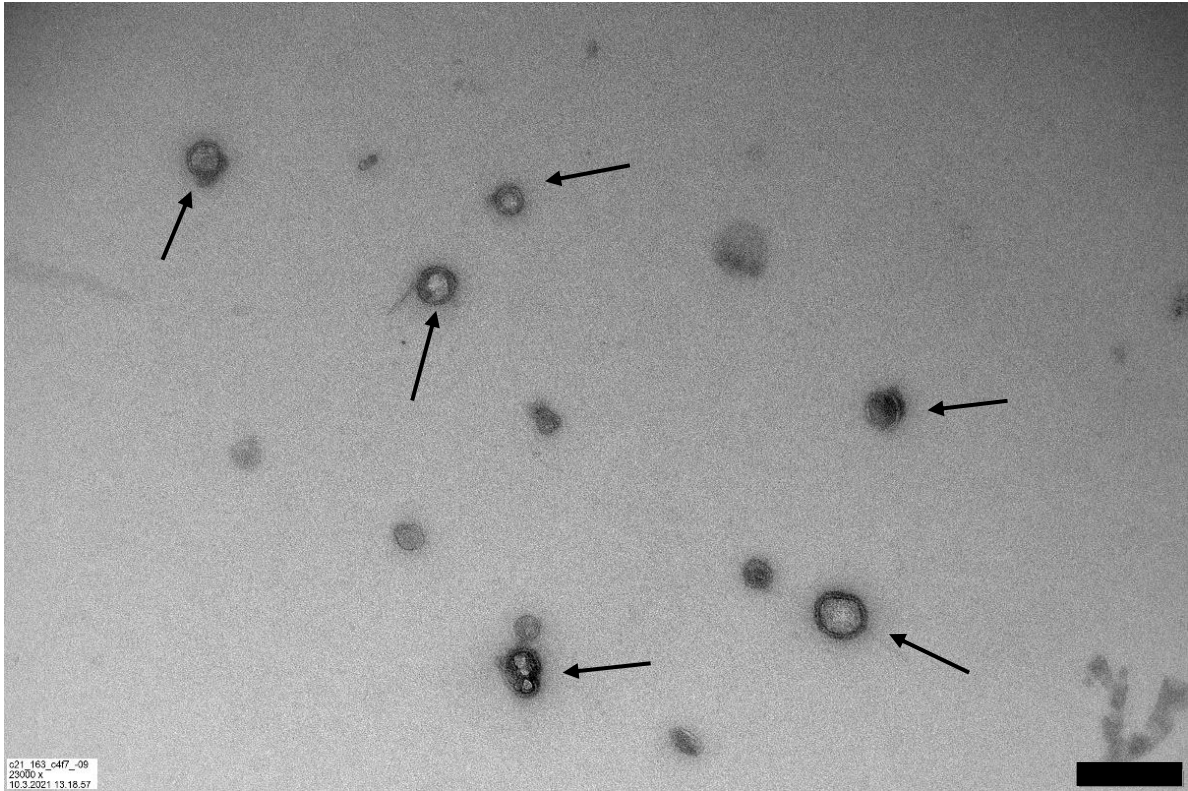


Figure 2. Negative-stained BEVs from isolation round 2 in TEM. Characteristic features of EVs include round shape, size between 20–500 nm and visible bilayer membrane (arrows). Scalebar 200 nm.

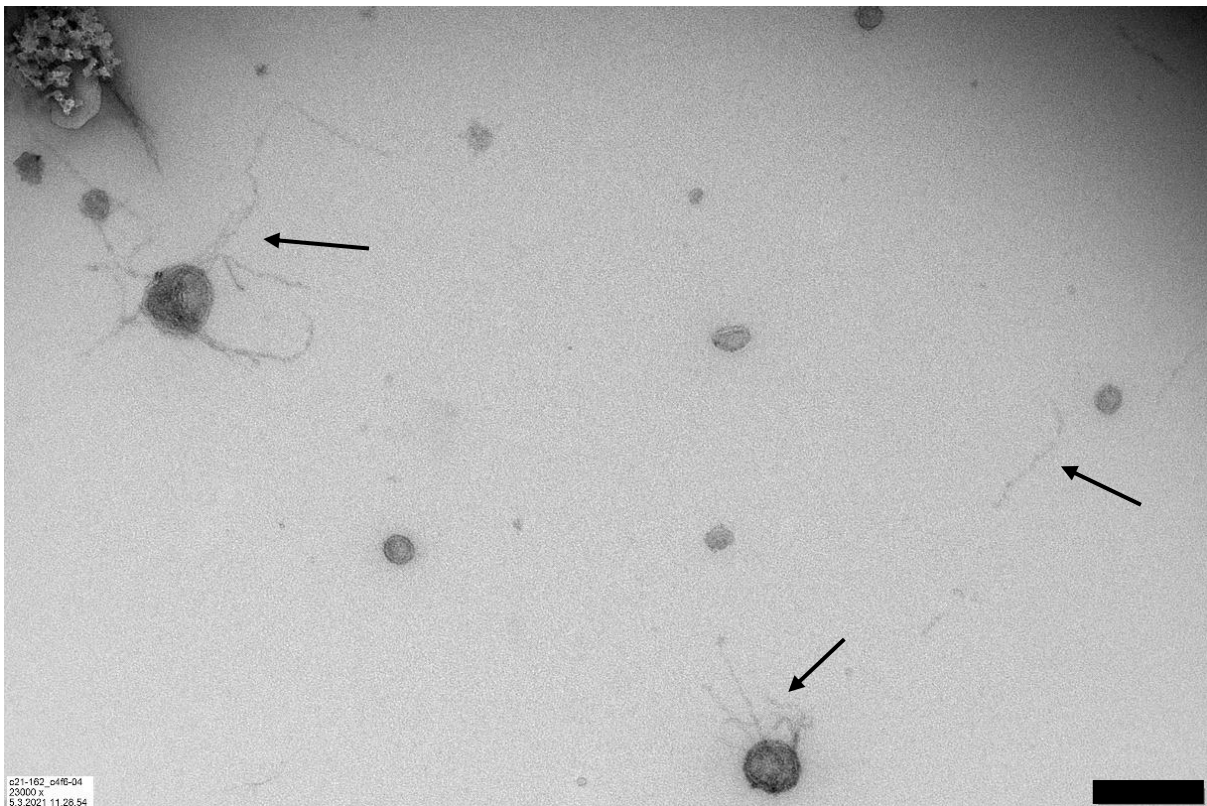


Figure 3. Negative-stained BEVs from isolation round 2 in TEM. Filamentous structures among vesicles (arrows) are viral-, flagellar-, or pilin constructs. The amount of these constructs correlates with pureness of the sample. Scalebar 200 nm.

4.1.2. Nanoparticle tracking analysis

Aliquots for NTA were taken from the same fractions 6 and 7 (pooled) as used in TEM and measured individually and from mixtures of each round. Samples were diluted to PBS according to the output concentration of first 1:50 dilution (20 μ l sample + 980 μ l PBS) run in each sample. Minimum threshold value for samples was 5×10^7 particles/ml and maximum threshold value $8-9 \times 10^8$ particles/ml according to the manufacturer's instructions. The raw data is derived as nanoparticle size distribution graph (Figure 4).

Actual concentrations of samples were calculated by multiplying the raw data concentration with the dilution factor (Table 4). Particle size distribution is displayed with mean, mode, D10, D50 and D90 -values. In D10, 10 % of the analyzed particles are below the given value (size in nanometers). Similarly, in D50, 50 % and in D90, 90 % of the analyzed particles are below the given value.

In these samples, most of the particles are from 100 to 300 nm in size, which is visible from the graph and in accordance with D10–D90 values.

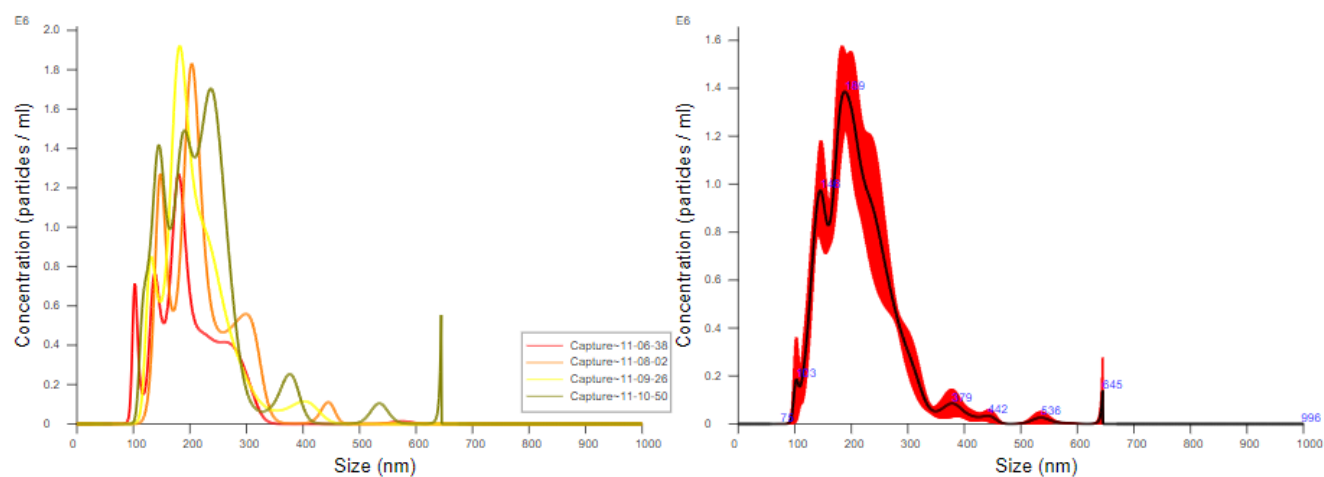


Figure 4. Data of the final mixture of all samples (rounds 2–4) measured with NTA (Nanosight NS300). Concentration by particle size of different captures on the same run (left). Averaged concentration through different captures by particle size (right).

Table 4. NTA measurement data for BEVs isolated from human fecal samples. Five human fecal samples (C2, C4, C6, C9, and C12) were used in four independent rounds (1–4).

Sample	Raw data conc (particles/ml)	Dilution factor	Actual conc (particles/ml)	Mean (nm)	Mode (nm)	D10 (nm)	D50 (nm)	D90 (nm)
Round 1								
C2.1	8.20E+07	25	2.05E+09	158.9	149.4	115.0	151.9	225.1
C4.1	8.31E+09	25	2.08E+11	221.9	155.4	143.9	212.0	308.6
C6.1	3.86E+07	25	9.65E+08	195.4	163.2	115.0	177.1	279.2
C9.1	3.29E+08	25	8.23E+09	223.3	162.4	138.0	204.1	318.3
Round 2								
C2.2	3.09E+08	25	7.73E+09	198.5	140.4	127.8	173.5	303.8
C4.2	1.12E+09	25	2.80E+10	213.7	174.3	142.3	200.7	294.0
C6.2	1.11E+08	50	5.55E+09	179.9	153.8	110.3	161.9	251.5
C9.2	2.65E+08	50	1.33E+10	222.6	175.7	135.4	196.7	349.6
C12.2	1.09E+08	50	5.45E+09	193.2	113.5	115.2	174.8	301.2
mix 2 (all)	2.33E+08	50	1.17E+10	213.7	198.2	137.8	198.1	295.8
Round 3								
C2.3	1.33E+08	50	6.65E+09	215.9	133.4	127.6	188.9	343.1
C4.3	9.45E+08	50	4.73E+10	231.3	206.6	159.0	219.9	309.0
C6.3	1.12E+08	50	5.60E+09	172.1	125.0	110.4	168.4	251.1
C9.3	4.08E+08	50	2.04E+10	238.2	205.5	145.3	211.4	354.0
C12.3	9.43E+07	50	4.72E+09	206.6	130.0	118.4	181.5	329.8
mix 3 (all)	5.32E+08	50	2.66E+10	221.1	198.4	137.2	201.9	316.3
Round 4								
C2.4	1.33E+08	50	6.65E+09	164.0	104.2	100.8	139.6	244.7
C4.4	2.32E+08	50	1.16E+10	229.5	175.6	169.9	210.4	311.3
C6.4	1.05E+08	50	5.25E+09	165.2	174.3	109.9	163.9	219.6
C9.4	2.18E+08	50	1.09E+10	259.0	213.4	155.5	232.3	391.0
C12.4	1.02E+08	50	5.10E+09	187.4	124.9	107.0	160.6	278.6
mix 4 (all)	2.35E+08	50	1.18E+10	237.4	200.3	159.5	214.9	326.4
mix all (rounds 2–4)	1.75E+08	50	8.75E+09	212.3	188.4	140.3	203.1	291.3

Concentrations of the samples from the first isolation rounds were lower than in the other three rounds and thus the first preparation was not included to the final mixture. Therefore, the mixture of all samples represents a pool of samples from rounds 2, 3 and 4 (Figure 4).

In this study, TEM was used to confirm the success of isolation procedure. NTA was performed to estimate concentration as sizes of particles in samples.

4.1.3. Protein concentration measurements

The amount of protein was measured from the same fractions 6 and 7 (pooled) of each sample individually with two parallel spectrophotometric methods Nanodrop A280 and Nanodrop Pierce™ BCA (Table 5). In addition, a ratio of protein content per vesicle between Nanodrop and NTA data was counted.

In A280, measurement data is much less variable compared to Pierce™ BCA. The values of A280 measurement varied between 22.95 µg/ml (C4.1) and 48.11 µg/ml (C2.3). In Pierce™ BCA, values varied from 5.01 µg/ml (C6.1) to 3729.56 µg/ml (C4.3). Protein concentration from sample C6 in last two rounds in Pierce™ BCA was too low to be detected, and the concentration of mixture of all samples too high to be detected even after preparing a higher standard curve (1000–2000 µg/ml). Therefore, ratio between Pierce™ BCA and NTA is not available for these three samples.

Table 5. Protein concentration data from Nanodrop A280 and Nanodrop Pierce™ BCA measurements for each round including counted ratios with NTA data (for NTA, see Table 1).

Sample	A280		Pierce™ BCA	
	Protein conc (µg/ml)	Ratio A280/NTA (µg/particle)	Protein conc (µg/ml)	Ratio Pierce/NTA (µg/particle)
Round 1				
C2.1	23.71	1.16E-05	9.45	4.61E-09
C4.1	22.95	1.10E-07	101.75	4.90E-10
C6.1	25.74	2.67E-05	5.01	5.19E-09
C9.1	38.03	4.62E-06	19.57	2.38E-09
Round 2				
C2.2	38.87	5.03E-06	77.36	1.00E-08
C4.2	35.12	1.25E-06	2672.47	9.54E-08
C6.2	40.87	7.36E-06	27.12	4.89E-09
C9.2	43.24	3.26E-06	182.33	1.38E-08
C12.2	35.81	6.57E-06	133.59	2.45E-08
mix 2 (all)	34.21	2.94E-06	648.71	5.57E-08
Round 3				
C2.3	48.11	7.23E-06	92.49	1.39E-08
C4.3	43.27	9.16E-07	3729.56	7.89E-08
C6.3	42.86	7.65E-06	ND (out of range: low)	N/A
C9.3	34.15	1.67E-06	433.56	2.13E-08
C12.3	28.21	5.98E-06	134.65	2.86E-08
mix 3 (all)	42.10	1.58E-06	1772.83	6.66E-08
Round 4				
C2.4	33.59	5.05E-06	127.5	1.92E-08
C4.4	26.95	2.32E-06	736.43	6.35E-08
C6.4	28.98	5.52E-06	ND (out of range: low)	N/A
C9.4	33.43	3.07E-06	179	1.64E-08
C12.4	40.45	7.93E-06	31.45	6.17E-09
mix 4 (all)	34.51	2.94E-06	167.26	1.42E-08
mix all (2–4)	39.68	4.54E-06	ND (out of range: high)	N/A

4.2. HRP-labeling

HRP-labeling protocol was tested through different conditions listed (Table 6).

Table 6. Summary of different conditions and negative controls tested for DAB-reaction. Conditions 9 and 10 were negative stained and therefore not listed in this table. RT = room temperature

Condition	1 % glutaraldehyde fixation	1 % osmium and 1.5 % potassium ferrocyanide (time and temperature of incubation)	Uranylacetate (UA) coating
1	X	60min +4 °C	X
2	X	30min RT	X
3		60min +4 °C	X
4		30min RT	X
5	X	60min +4 °C	
6	X	30min RT	
7 (negative control)	X	30min RT	
8 (negative control)	X	30min RT	
11 (negative control)		30min RT	X
12 (negative control)		30min RT	X
13 (negative control)		30min RT	X
14 (negative control)	X	30min RT	X

In conditions 1 and 2, both glutaraldehyde and UA were used. Vesicle-resembling structures were mostly present, but the background was grainy (Figure 5). There was no clear difference seen between the different incubation times and temperatures. Some differences were seen between the same condition in different trials (Figure 5, Figure 6).

In conditions 3 and 4, vesicle-like structures were present, appearing with dark, sharply stained edges, considered to result from HRP-labeling (Figure 7, Figure 8). There was still some graininess in the background. Incubation time and temperature did not noticeably affect the results.

In conditions 5 and 6 the concentration of vesicle-like particles was very low, and the background was grainy and the overall look shady (Figures 9 and 10). Some sharp-stained structures were seen in condition 11 of trial 3 (Figure 11).

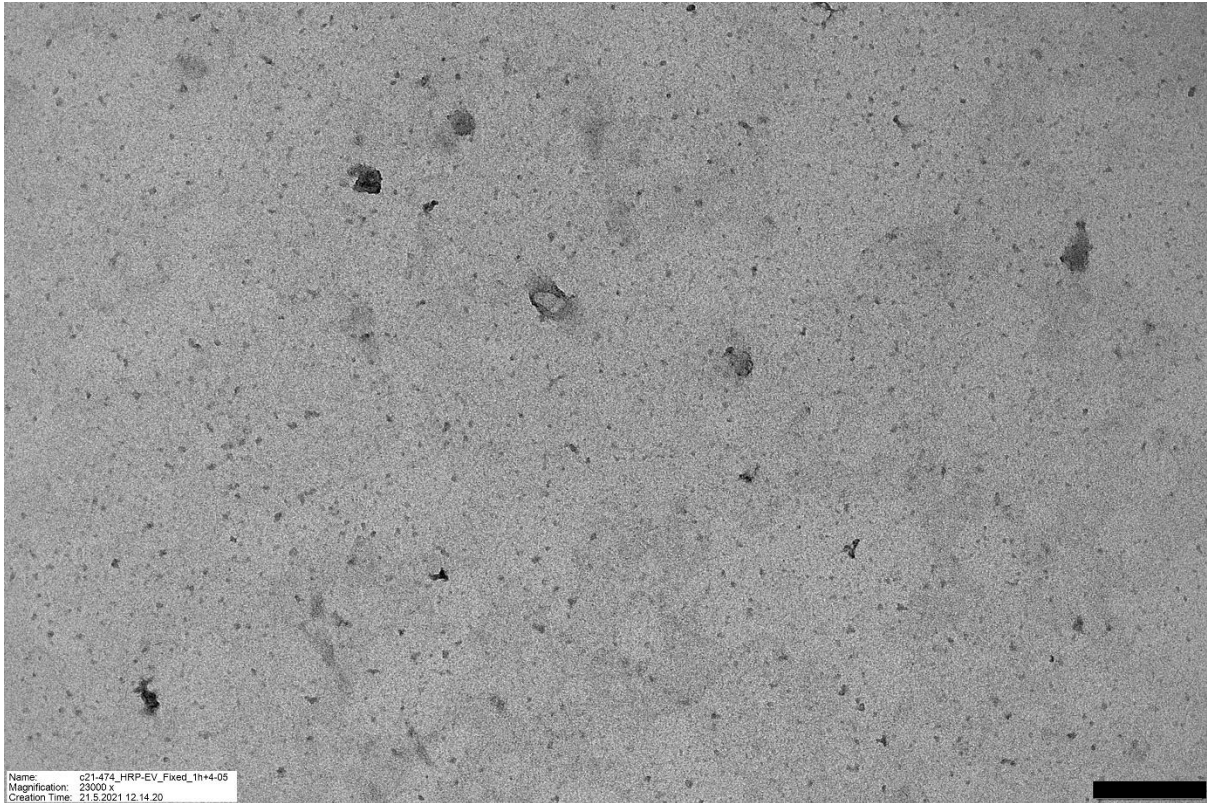


Figure 5. Condition 1 (trial 1). HRP-labeled BEVs, fixed with glutaraldehyde, UA-coating, osmium incubation 60 min at +4 °C. Grainy background with a few vesicle-resembling structures. Scalebar 200 nm.

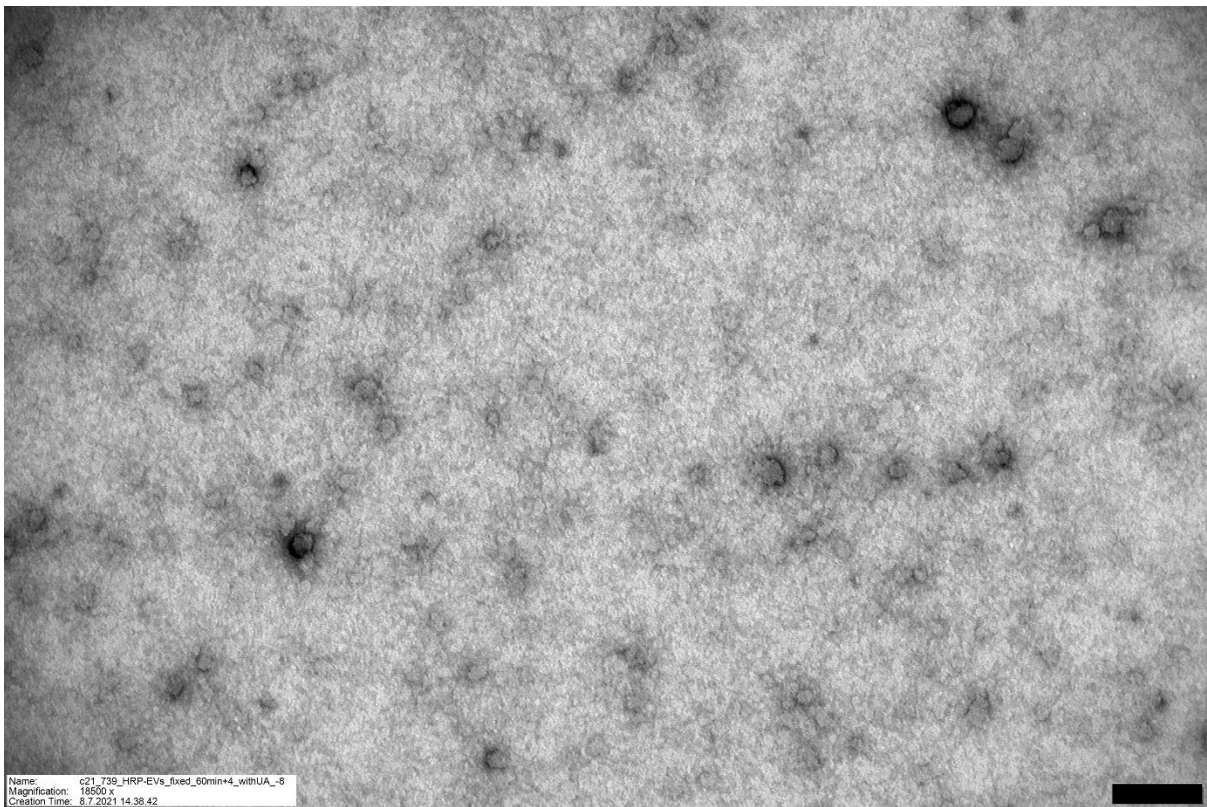


Figure 6. Condition 1 (trial 3). HRP-labeled BEVs, fixed with glutaraldehyde, UA-coating, osmium incubation 60 min at +4 °C. Shady overall look with some vesicle-resembling structures. Scalebar 200 nm.

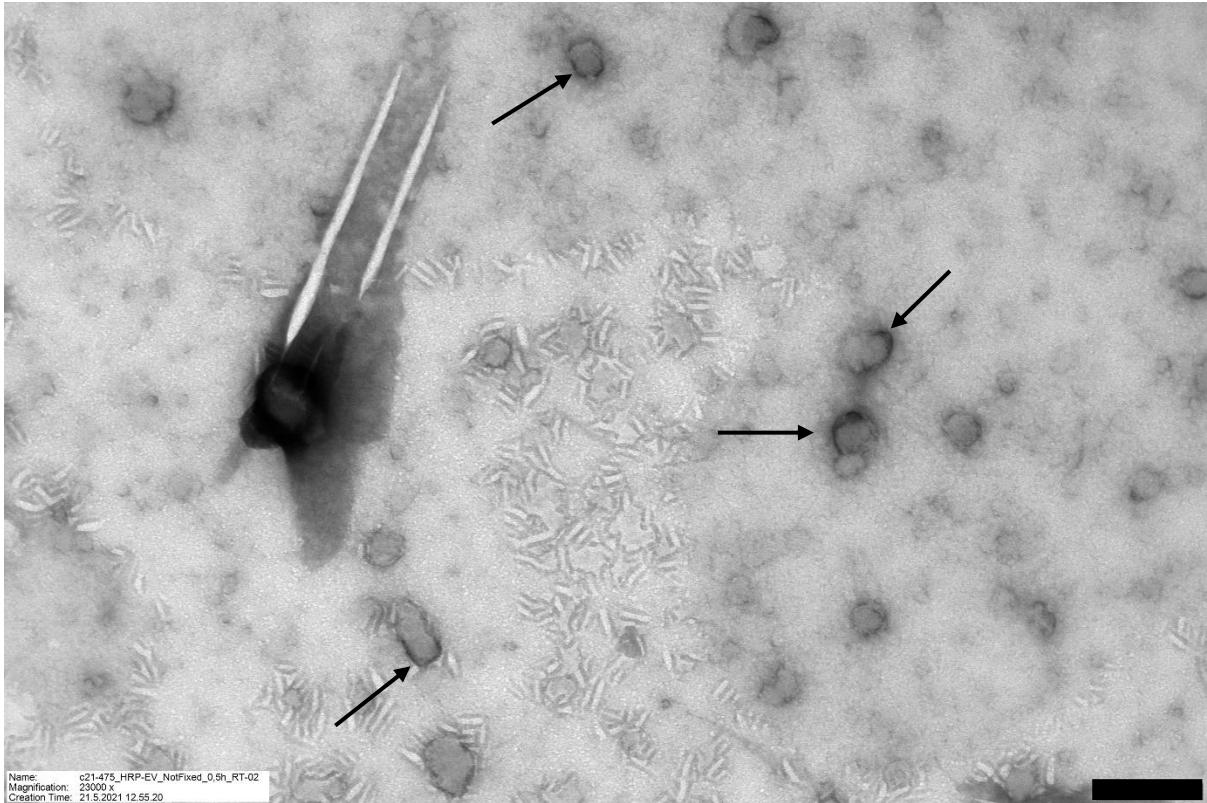


Figure 7. Condition 4 (trial 1). HRP-labeled BEVs, UA-coating, osmium incubation 30 min at RT. Vesicle-resembling structures with sharp-stained edges visible (arrows). Scalebar 200 nm.

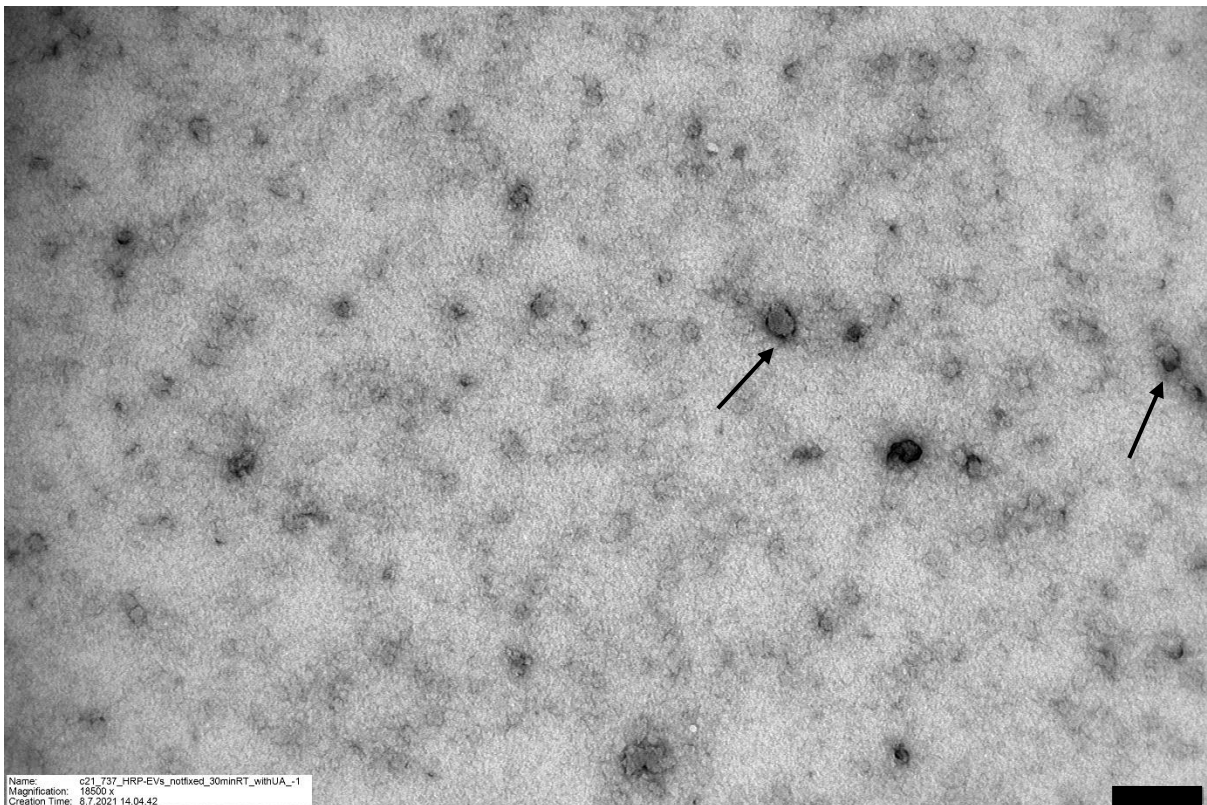


Figure 8. Condition 4 (trial 3). HRP-labeled BEVs, UA-coating, osmium incubation 30 min at RT. Vesicle-resembling structures with sharp-stained edges visible (arrows). Scalebar 200 nm.

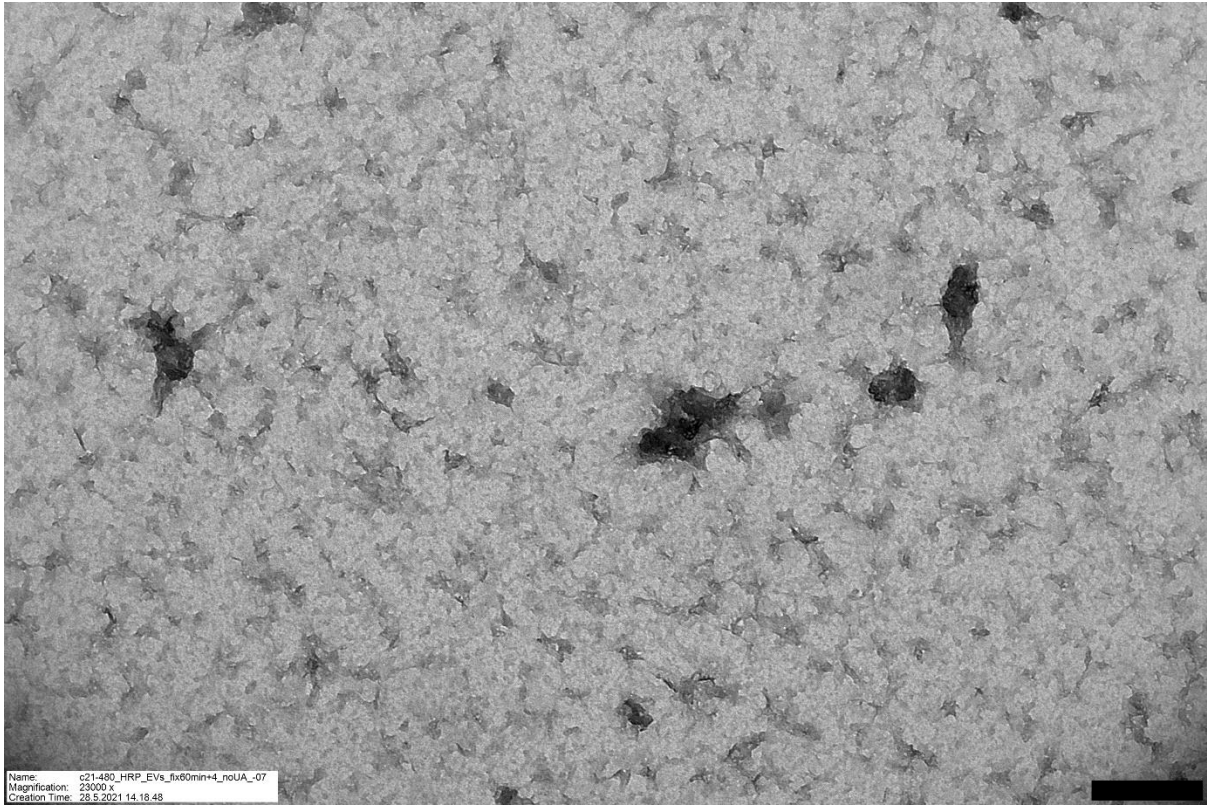


Figure 9. Condition 5 (trial 2). HRP-labeled BEVs, fixed with glutaraldehyde, osmium incubation 60 min at +4 °C. Shady overall look, no clear vesicle-resembling structures present. Scalebar 200 nm.

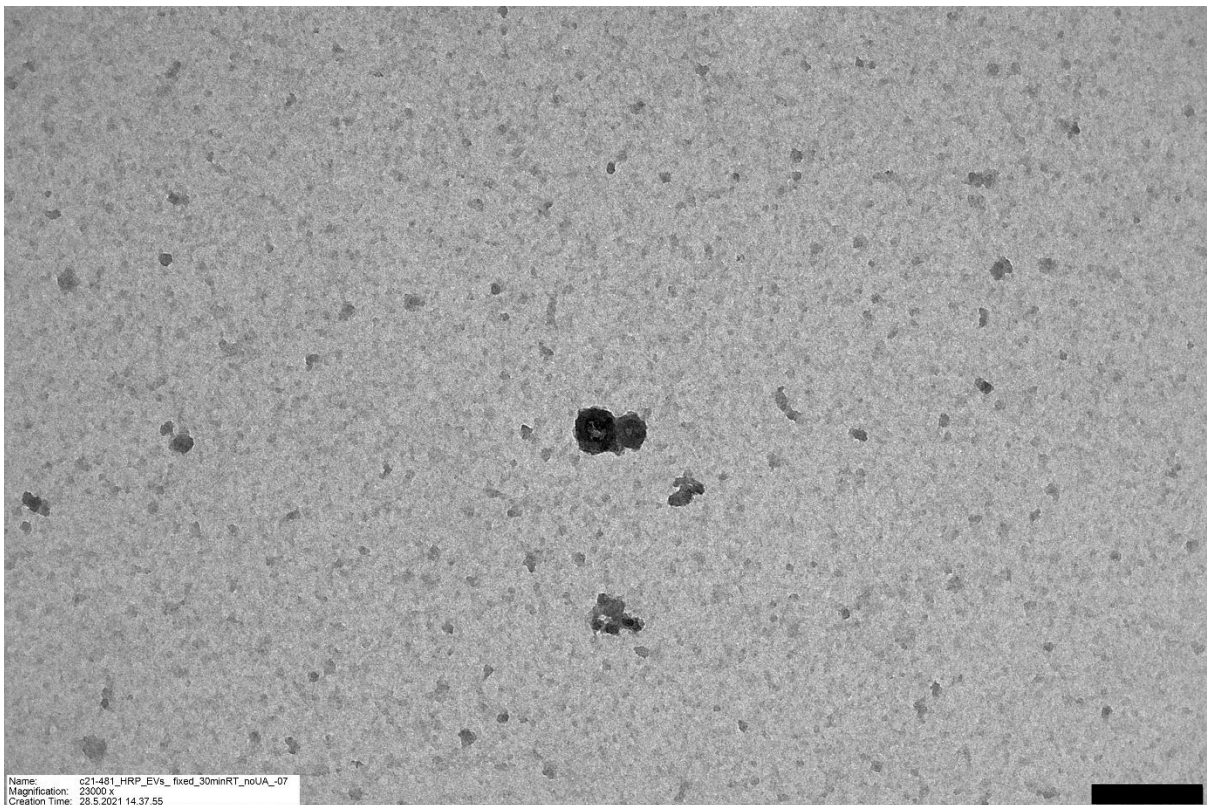


Figure 10. Condition 6 (trial 2). HRP-labeled BEVs, fixed with glutaraldehyde, osmium incubation 30 min at RT. Grainy background, no clear vesicle-resembling structures present. Scalebar 200 nm.

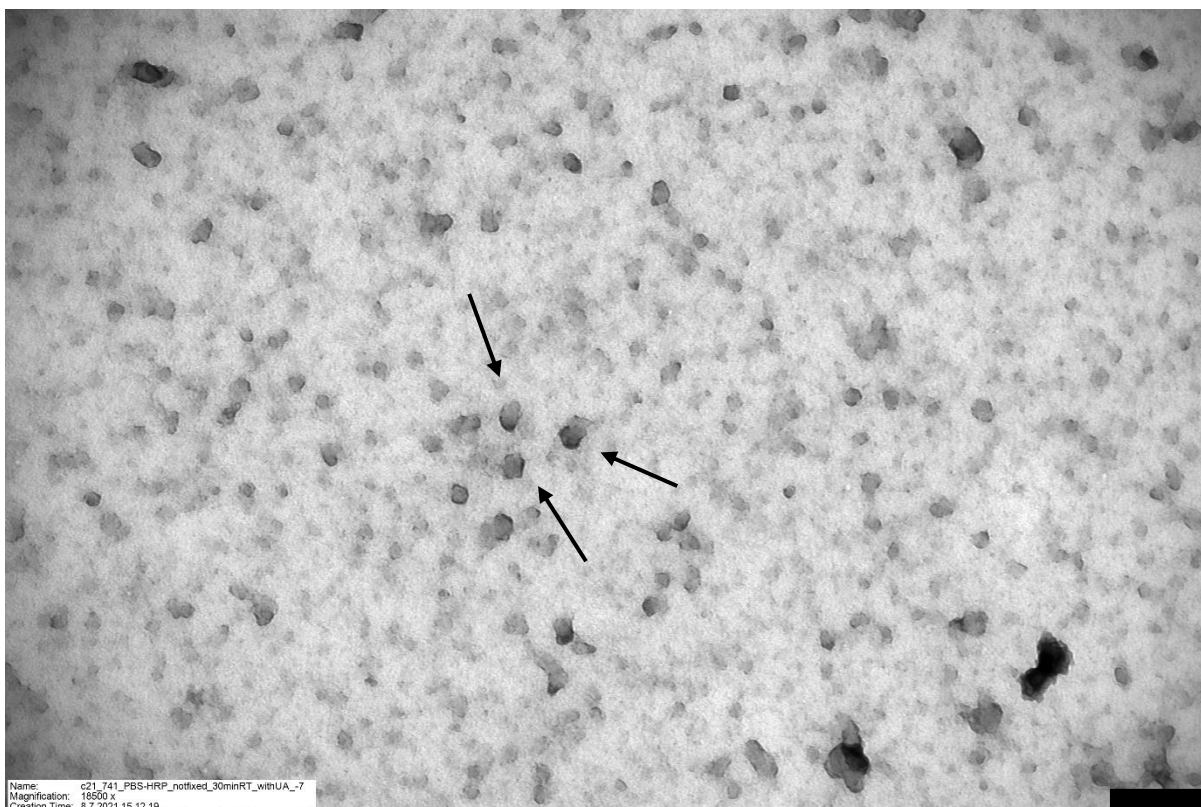


Figure 11. Condition 11 (trial 3). HRP-labeled PBS (negative control), UA-coating, osmium incubation 30 min at RT. Structures with sharp-stained edges visible (arrows). Scalebar 200 nm.

4.3. *Ex vivo* mouse experiment

Finally, HRP-labeling and DAB-reaction for BEVs was tested *ex vivo* with two muscle injections to a euthanized mouse. After plastic embedding and thin sectioning, the samples were ready for imaging in TEM.

Vesicle-like structures were seen in clusters in muscle samples 1 and 2 (HRP-labeled BEVs) (Figures 12 and 13) as assumed. However, these structures were seen also outside the sample area in sample 1 (Figure 14). Vesicle-resembling particles were seen also in muscle sample 3 (maleimide-incorporated BEVs without HRP) and muscle sample 4 (maleimide-incorporated BEVs without HRP and DAB) (Figures 15 and 16). In HRP-labeled samples 1 and 2, vesicle-resembling structures appear slightly darker than in samples 3 and 4 with maleimide only. In plain muscle samples 5 and 6 no vesicle-like structures were seen (Figure 17).

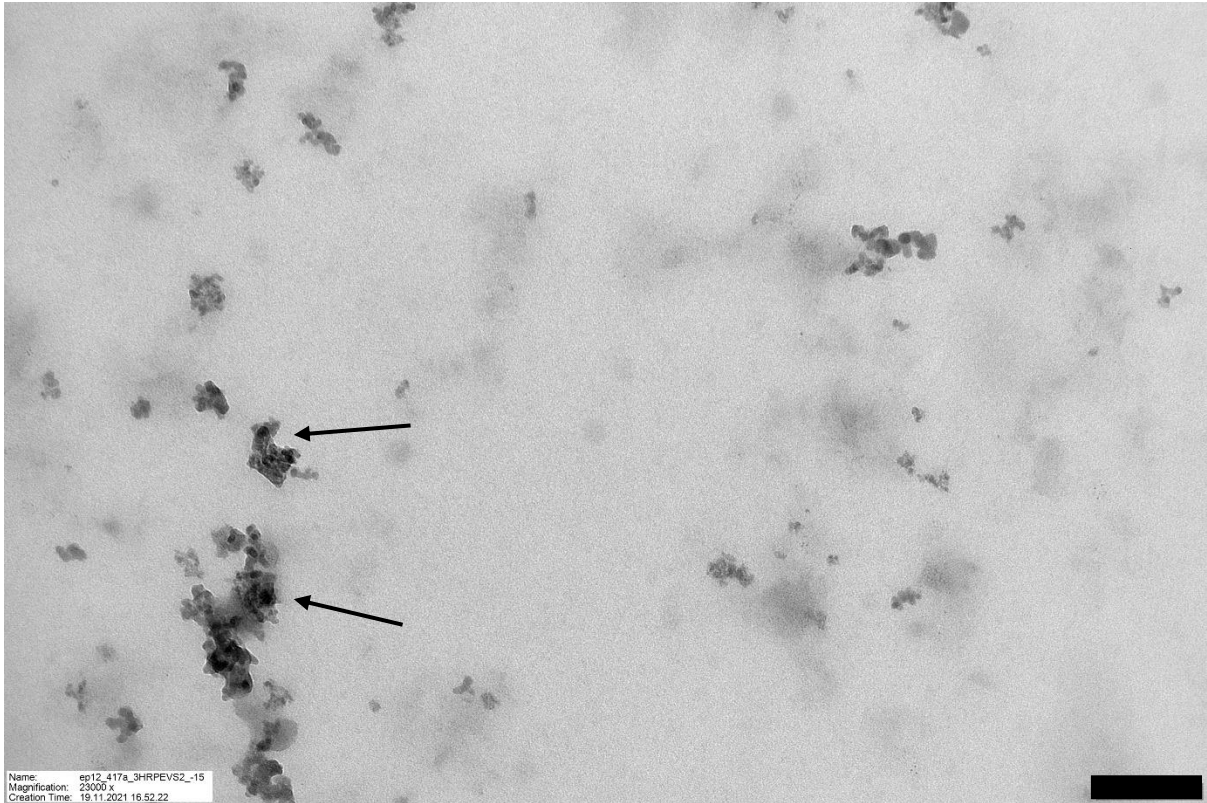


Figure 12. Muscle sample 1: HRP-labeled BEVs in mouse muscle tissue. Dark-stained vesicle-resembling structures appear in clusters (arrows). Scalebar 200 nm.

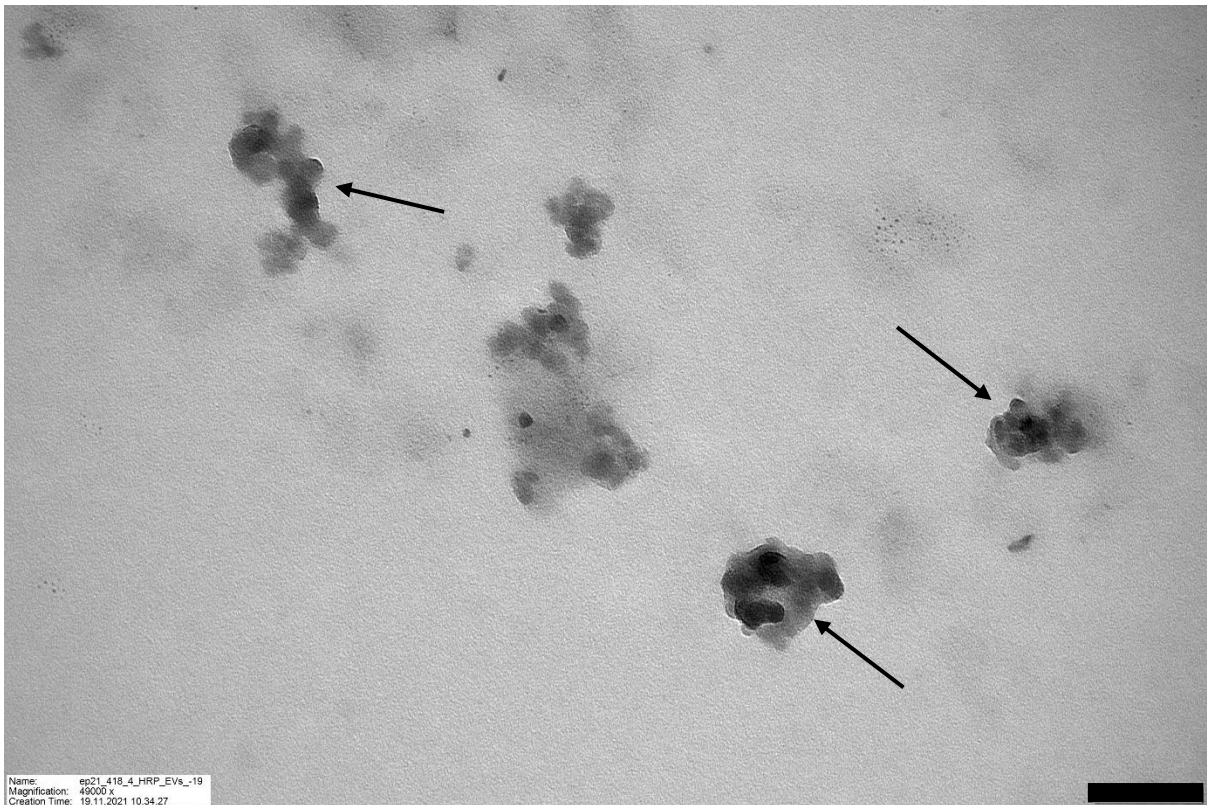


Figure 13. Muscle sample 2: HRP-labeled BEVs in mouse muscle tissue. Vesicle-resembling structures in clusters with dark staining and visible bilayer (arrows). Scalebar 100 nm.

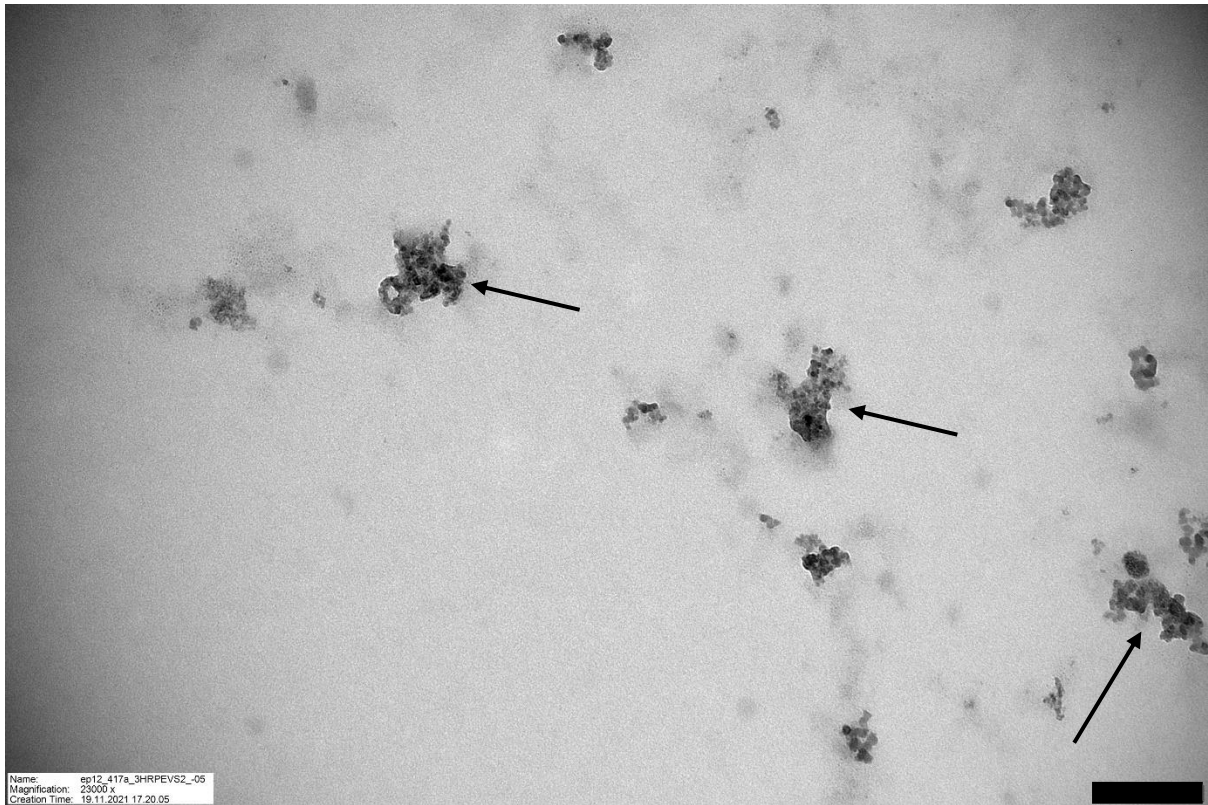


Figure 14. Muscle sample 1: HRP-labeled BEVs in mouse muscle tissue (outside the sample area). Here BEV-resembling structures (arrows) appear also in the coating of the sample. Scalebar 200 nm.

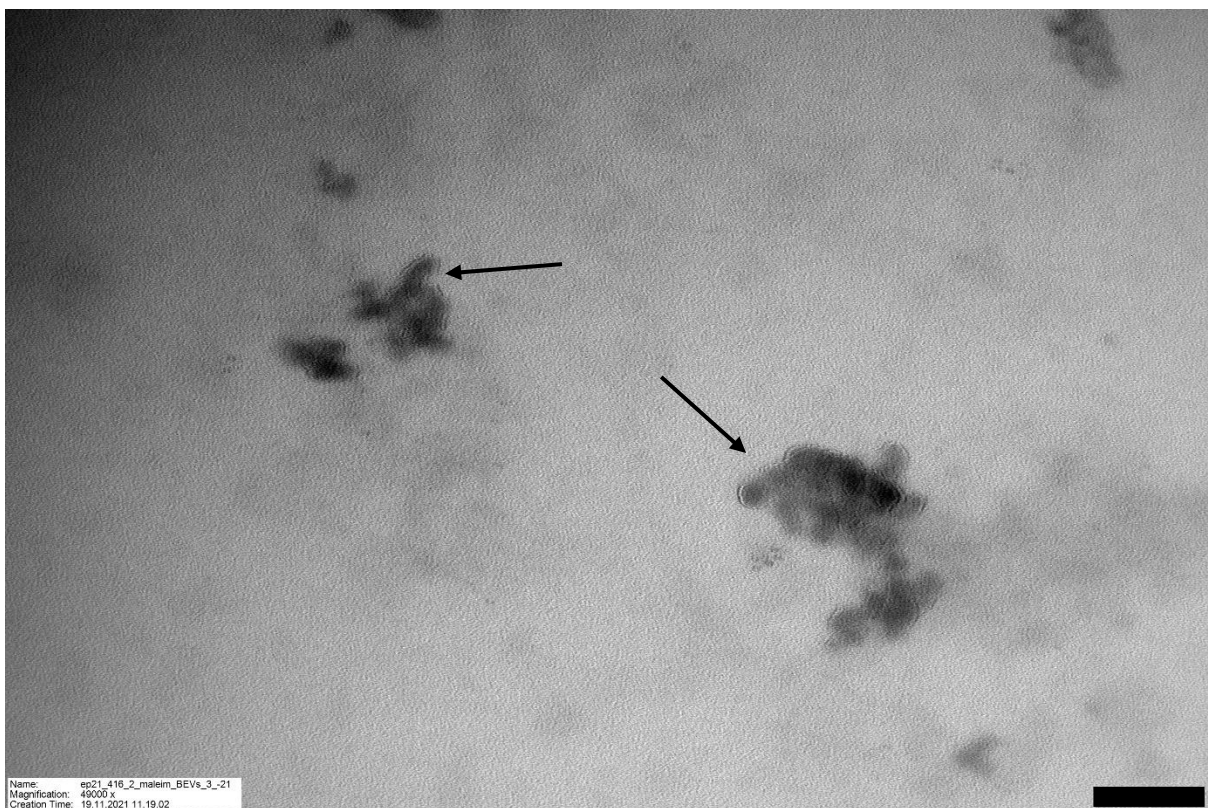


Figure 15. Muscle sample 3: Maleimide-incorporated BEVs with DAB-reaction. Vesicle-resembling structures with bilayers are visible (arrows) but seem slightly lighter compared to HRP-labeled ones. Scalebar 100 nm.

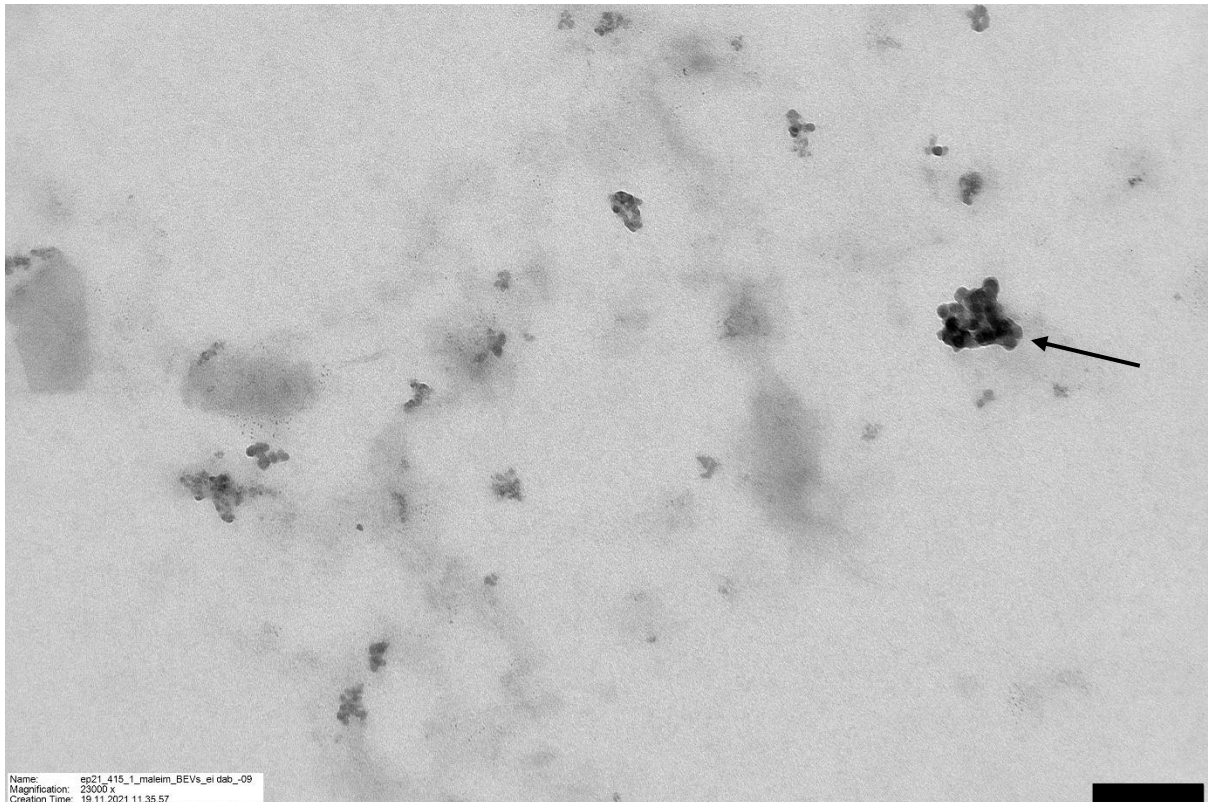


Figure 16. Muscle sample 4: Maleimide-incorporated BEVs without DAB-reaction. Vesicle-resembling structures are visible (arrow) but seem slightly lighter compared to HRP-labeled ones. Scalebar 200 nm.

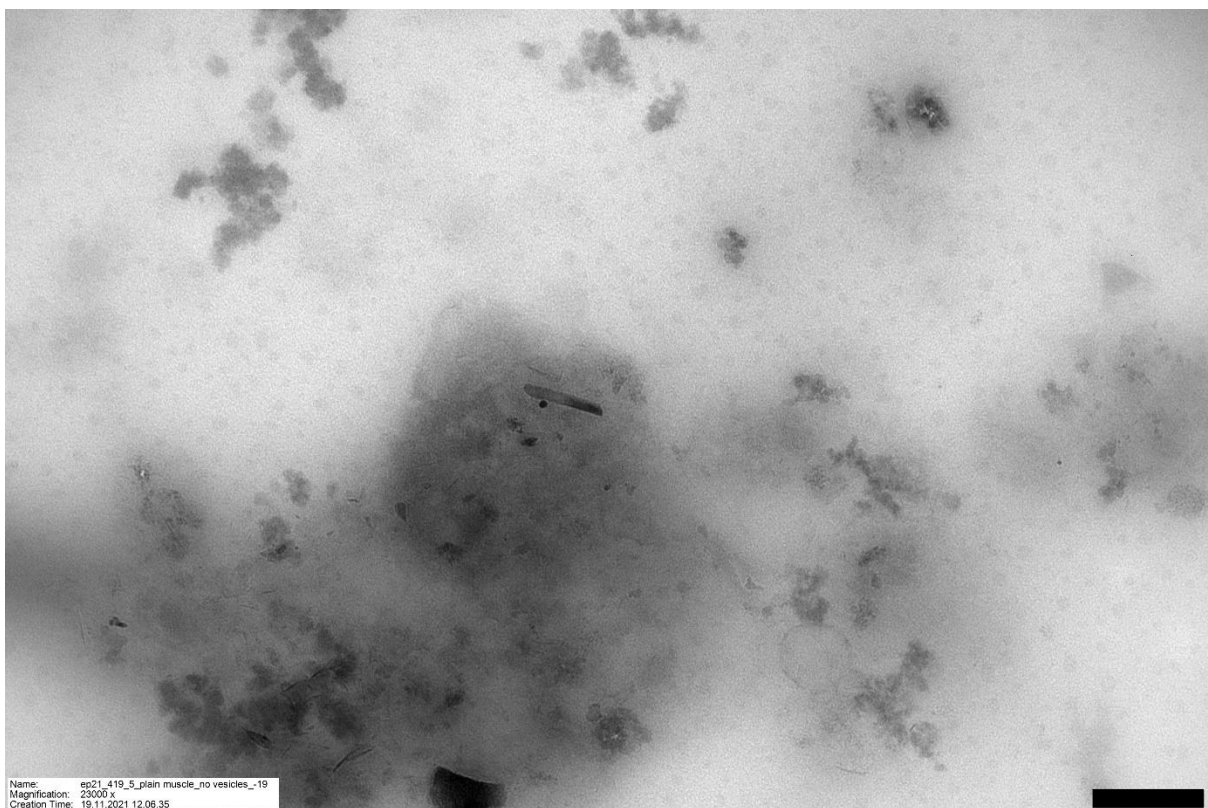


Figure 17. Muscle sample 5: Plain muscle sample without BEVs. No clusters of vesicle-resembling structures present. Scalebar 200 nm.

5. Discussion

Tracking EV drift or penetration in tissues on cellular level has not been achieved yet. Coming up with a novel labeling method, a higher level of resolution could be achieved via TEM imaging of EVs. The possibility to track the EV distribution through human body could offer deeper knowledge of the EV and BEV functions and promote their use in clinical applications or as disease markers. The aim of this thesis was to establish a novel labeling method for BEVs to be used for visualizing samples in TEM. Labeling was first established *in vitro*, and then verified *ex vivo* after labeled vesicles were injected into mouse.

In *in vitro* setup on the grids, the best-looking staining was achieved with UA-coating without application of glutaraldehyde. Duration and temperature of osmium incubation did not remarkably affect the outcome, although 30-minute incubation at room temperature gave more reproducible results between different trials. During the successful HRP-labeling, EV-resembling structures in the samples appeared sharply stained on the edges. In addition to BEV-samples, some sharp staining was seen in one of the negative control samples, where PBS was used during HRP-coupling procedure instead of BEVs. This suggests that round, sharply stained structures partially represent some staining artefacts as well.

In the DAB-reaction, glutaraldehyde acts as a fixative whereas UA is used as a stain for creating contrast in TEM-imaging. In HRP-labeling, the contrast that UA creates is so strong that it can hide other features, like the dark-stained DAB-polymer, underneath it. In some samples, glutaraldehyde and UA-coating were used together, resulting in graininess in the background of the sample in TEM. This graininess together with some aggregates, presumably from fixatives and coating, left the BEVs unseen in some of the samples. In other samples, either glutaraldehyde or UA was used. Glutaraldehyde-fixation seemed to give higher background compared to UA-coating, when used individually. Altogether, graininess in the background complicated the imaging in TEM, making it harder to distinguish vesicles from other material in the samples.

The optimal condition established, HRP-labeled BEVs with UA-coating and incubation with osmium for 30 minutes at room temperature, was further tested in an animal model. In *ex vivo* conditions, clusters of dark, vesicle-resembling structures were seen in samples with HRP-labeled BEVs. Dark-stained clusters seemed to hold round-shaped particles with bilayers. In negative control samples without HRP, or without HRP and DAB, these clusters appeared

slightly lighter compared to labeled ones. Clusters were missing in control samples with HRP-stained PBS, suggesting that these structures could be holding BEVs. Nevertheless, in one HRP-BEV-sample similar structures were found outside the thin section, from the coating. This indicates that dark structures in this particular sample are likely artefacts from the preparation of the sample.

In this labeling, osmium complicates the identification of BEVs in tissues. In TEM imaging, differences in contrast are essential and formed using stains containing heavy metals, here osmium. The polymer of DAB is osmiophilic, meaning that osmium used in the reaction binds to DAB, appearing dark in TEM. Since osmium binds to the lipid-containing membranes in the samples as well, it is difficult to distinguish, if structures with osmium are vesicles or other membranous particles. In further tests of HRP-labeling, other heavy metals could be examined and possibly tested instead of osmium. Other reagents might still bind to somewhere else in the sample and could be considered for further protocol optimization.

Multiple trials were tested *in vitro* with some variation in the results. The variation can partially appear from the inexperience of the researcher to work with grids during sample preparation for TEM. Mouse experiment was done with one mouse and only two parallel samples because of limited timeframe of this thesis. For achieving more reliable results, more trials in both *in vitro* and *ex vivo* conditions should be done.

In addition to HRP-labeling, different characterization methods for EVs were performed and compared. Results between the two protein concentration measurement assays, A280 and Pierce™ BCA, varied between the samples when compared to each other. Of these methods, Pierce™ BCA assay seems to give more variable values compared to A280 through individuals. Data scatter is highly reproducible in different isolation rounds and is therefore considered to reflect the properties of individual samples. The data suggest that Pierce™ BCA assay is more reliable way to estimate protein concentration in EV preparations in comparison with A280 measurement. Results of the NTA and Pierce™ BCA protein concentrations go hand in hand. The ratio of protein concentration measured by Pierce™ BCA to the particle amount measured by NTA is to some extent similar in individual samples, which is expected.

6. Conclusions

Results of the current thesis suggest a novel labeling protocol for labeling BEVs with HRP suitable for TEM imaging. The best condition for HRP-labeling *in vitro* included uranyl acetate and osmium incubation. Further *ex vivo* and *in vivo* studies are needed to optimize the current protocol to be suitable for mouse work. Some modifications of the protocol as well as alternative heavy metals can be considered.

Acknowledgements

I would like to thank my supervisors Justus Reunanen, Nadiya Byts, Mika Kaakinen and Lumi Viljakainen from University of Oulu for all the help and advice. I would also like to thank research group members Sonja Salmi, Jenni Hekkala and Surbhi Mishra and the EM Core laboratory staff for helping me with the lab work at Biocenter Oulu. I wish to thank my family and friends for the support.

References

- Almeida S., Santos L., Falcão A., Gomes C., & Abrunhosa A. (2020) *In vivo* tracking of extracellular vesicles by nuclear imaging: advances in radiolabeling strategies. *International Journal of Molecular Sciences*, 21(24): 9443. doi: 10.3390/ijms21249443
- Altan-Bonnet N., & Chen Y.H. (2015) Intercellular transmission of viral populations with vesicles. *Journal of virology*, 89(24), 12242-12244. doi: 10.1128/JVI.01452-15
- Azevedo A.M., Martins V. C., Prazeres D. M., Vojinovic V., Cabral J. M. & Fonseca L. P. (2003) Horseradish peroxidase: a valuable tool in biotechnology. *Biotechnology annual review*, 9(3): 1387-2656. doi: 10.1016/S1387-2656(03)09003-3
- Badr C. E. & Tannous B. A. (2011) Bioluminescence imaging: progress and applications. *Trends in Biotechnology*, 29(12): 624-633. doi: i:10.1016/j.tibtech.2011.06.010
- Benedikter B.J., Bouwman F.G., Vajen T., Heinzmann, A., Grauls G., Mariman E.C., Wouters E., Savelkoul P.H., Lopez-Iglesias, C. Koenen, R. Rohde G. & Stassen F. (2017) Ultrafiltration combined with size exclusion chromatography efficiently isolates extracellular vesicles from cell culture media for compositional and functional studies. *Science Reports* 7: 15297. doi: 10.1038/s41598-017-15717-7
- Betzer, O., Perets, N., Angel, A., Motiei, M., Sadan, T., Yadid, G., Offen, D., & Popovtzer, R. (2017) *In vivo* neuroimaging of exosomes using gold nanoparticles. *ACS Nano*, 11(11), 10883–10893. doi: 10.1021/acsnano.7b04495
- Bitto, N.J., Chapman, R., Pidot, S., Costin A., Lo C., Choi J., D’Cruze T., Reynolds E.C., Dashper S.G., Turnbull L., Whitchurch C.B., Stinear T.P., Stacey K.J. & Ferrero R.L. (2017) Bacterial membrane vesicles transport their DNA cargo into host cells. *Science Reports* 7, 7072. doi: 10.1038/s41598-017-07288-4
- Brenner, S., & Horne, R. W. (1959) A negative staining method for high resolution electron microscopy of viruses. *Biochimica et biophysica acta*, 34: 103-110. doi: 10.1016/0006-3002(59)90237-9
- Busato A., Bonafede R., Bontempi P., Scambi I., Schiaffino L., Benati D., Malatesta M., Sbarbati A., Marzola P., & Mariotti R. (2016) Magnetic resonance imaging of ultrasmall superparamagnetic iron oxide-labeled exosomes from stem cells: a new method to obtain labeled exosomes. *International Journal of Nanomedicine*, 11: 2481–2490. doi: 10.2147/IJN.S104152
- Cao H., Yue Z., Gao H., Chen C., Cui K., Zhang K., Cheng Y., Shao G. Kong D., Li Z., Ding D. & Wang Y. (2019) *In vivo* real-time imaging of extracellular vesicles in liver regeneration via aggregation-induced emission luminogens, *ACS Nano*, 13(3): 3522–3533. doi: 10.1021/acsnano.8b09776
- Choi H. & Lee D.S. (2016) Illuminating the physiology of extracellular vesicles. *Stem Cell Research & Therapy* 7:55. doi: 10.1186/s13287-016-0316-1
- Conde-Vancells J., Rodriguez-Suarez E., Embade N., Gil D., Matthiesen R., Valle M., & Falcon-Perez, J. M. (2008) Characterization and comprehensive proteome profiling of

exosomes secreted by hepatocytes. *Journal of Proteome Research* 7(12): 5157-5166. doi: 10.1021/pr800488

Ellis E.A. (2014) Staining sectioned biological specimens for transmission electron microscopy: conventional and en bloc stains. In *Electron Microscopy* (pp. 57-72). Humana Press, Totowa, NJ.

Fevrier B., Vilette D., Archer F., Loew D., Faigle W., Vidal M., Laude H. & Raposo G. (2004) Cells release prions in association with exosomes. *Proceedings of the National Academy of Sciences*, 101(26): 9683-9688. doi: 10.1073/pnas.0308413101

Frühbeis C., Fröhlich D., Kuo W. P., Amphornrat J., Thilemann S., Saab A.S., Kirchhoff F., Möbius W., Goebbels S., Nave K. A., Schneider A., Simons M., Klugmann M., Trotter J. & Krämer-Albers E.M. (2013) Neurotransmitter-Triggered Transfer of Exosomes Mediates Oligodendrocyte–Neuron Communication. *PLOS Biology* 11(7): e1001604. doi: 10.1371/journal.pbio.1001604

Gangadaran P., Li X.J., Lee H.W., Oh J.M., Kalimuthu S., Rajendran R.L., Son S.H., Singh T. D, Zhu L., Jeong S.Y., Lee S., Lee J. & Byeong-Cheol A. (2017) A new bioluminescent reporter system to study the biodistribution of systematically injected tumor-derived bioluminescent extracellular vesicles in mice. *Oncotarget*, 8:109894-109914. doi: 10.18632/oncotarget.22493

Gill S., Catchpole R. & Forterre, P. (2018) Extracellular membrane vesicles in the three domains of life and beyond. *FEMS Microbiology Reviews*, 43(3): 273–303 doi: 10.1093/femsre/fuy042

Guerrero-Mandujano A., Hernández-Cortez C., Ibarra J.A., & Castro-Escarpulli G. (2017) The outer membrane vesicles: secretion system type zero. *Traffic*, 18(7): 425-432. doi: 10.1111/tra.12488

Gurunathan S., Kang, M-H., Jeyaraj, M., Qasim, M & Kim, J-H. (2019) Review of the Isolation, Characterization, Biological Function, and Multifarious Therapeutic Approaches of Exosomes. *Cells*, 8(4)307 doi: 10.3390/cells8040307

Hayat, M.A. (1986) Glutaraldehyde: role in electron microscopy. *Micron and Microscopica Acta*, 17(2): 115-135. doi: 10.1016/0739-6260(86)90042-0

Hoshino A., Costa-Silva B., Shen T.L., Rodrigues G., Hashimoto A., Mark M.T., Molina H., Kohsaka S., Di Giannatale A., Ceder S., Singh S., Williams C., Sopolop N., Uryu K., Pharmed L., King T., Bojmar L., Davies A.E., Ararso Y., ... & Lyden, D. (2015) Tumour exosome integrins determine organotropic metastasis. *Nature*, 527: 329–335. doi: /10.1038/nature15756

Hu L., Wickline S.A. & Hood J.L. (2015) Magnetic resonance imaging of melanoma exosomes in lymph nodes. *Magnetic Resonance in Medicine*, 74: 266-271. doi: 10.1002/mrm.25376

Ingato D., Edson J.A., Zakharian M. & Kwon Y.J. (2018) Cancer cell-derived, drug-loaded Nanovesicles induced by sulfhydryl-blocking for effective and safe cancer therapy. *ACS Nano*, 12: 9568–9577. doi: 10.1021/acsnano.8b05377

- Jones E.J., Booth C., Fonseca S., Parker A., Cross K., Miquel-Clopés A., Hautefort I., Mayer U., Wileman T., Stentz R. and Carding S.R. (2020) the uptake, trafficking, and biodistribution of bacteroides thetaiotaomicron generated outer membrane vesicles. *Frontiers in Microbiology*, 11(57). doi: 10.3389/fmicb.2020.00057
- Kanada, M., Bachmann, M. H., Hardy, J. W., Frimannson, D. O., Bronsart, L., Wang, A., Sylvester M.D., Schmidt T.L., Kaspar R.L., Butte M.J., Matin A.C., & Contag, C. H. (2015) Differential fates of biomolecules delivered to target cells via extracellular vesicles. *Proceedings of the National Academy of Sciences*, 112(12): E1433-E1442. doi: 10.1073/pnas.1418401112
- Kim C.W., Lee H.M., Lee T.H., Kang C., Kleinman H.K., & Ghossein Y. S. (2002) Extracellular membrane vesicles from tumor cells promote angiogenesis via sphingomyelin. *Cancer research*, 62(21): 6312–6317. doi:
- Langlete P., Krabberød A.K & Winther-Larsen H.C. (2019) Vesicles from *Vibrio cholerae* contain AT-Rich DNA and shorter mRNAs that do not correlate with their protein products. *Frontiers in Microbiology* 10(2708). doi: 10.3389/fmicb.2019.02708
- Maas S., Breakefield X. & Weaver A. (2017) Extracellular vesicles: unique intercellular delivery vehicles. *Trends in Cell Biology*, 27(3): 172–188. doi: 10.1016/j.tcb.2016.11.003
- Matsumoto A., Takahashi Y., Nishikawa M., Sano K., Morishita M., Charoenviriyakul C., Saji H., & Takakura Y. (2017) Accelerated growth of B16BL6 tumor in mice through efficient uptake of their own exosomes by B16BL6 cells. *Cancer science*, 108(9): 1803–1810. doi: 10.1111/cas.13310
- Mizrak A., Bolukbasi M. F., Ozdener G. B., Brenner G. J., Madlener S., Erkan E. P., Ströbel T., Breakefield X. O., & Saydam O. (2013) Genetically engineered microvesicles carrying suicide mRNA/protein inhibit schwannoma tumor growth. *Molecular therapy: the journal of the American Society of Gene Therapy* 21(1): 101–108. doi: 10.1038/mt.2012.161
- Morishita M., Takahashi Y., Nishikawa M., Sano K., Kato K., Yamashita T., Imai T., Saji H. & Takakura Y. (2015) Quantitative analysis of tissue distribution of the B16BL6-derived exosomes using a streptavidin-lactadherin fusion protein and iodine-125-labeled biotin derivative after intravenous injection in mice. *Journal of pharmaceutical sciences*, 104(2): 705–713. doi: 10.1002/jps.24251
- Muralidharan-Chari V., Clancy J.W., Sedgwick A. & D'Souza-Schorey C. (2010) Microvesicles: mediators of extracellular communication during cancer progression. *Journal of Cell Science* 123(10): 1603–1611. doi: 10.1242/jcs.064386
- Nøkleby H., Aavitsland P., O'hallahan J., Feiring B., Tilman S., & Oster P. (2007) Safety review: two outer membrane vesicle (OMV) vaccines against systemic *Neisseria meningitidis* serogroup B disease. *Vaccine*, 25(16): 3080–3084. doi: 10.1016/j.vaccine.2007.01.022
- Pan S., Yang X., Jia Y., Li R., & Zhao R. (2014) Microvesicle-shuttled miR-130b reduces fat deposition in recipient primary cultured porcine adipocytes by inhibiting PPAR-g expression. *Journal of cellular physiology* 229(5): 631–639. doi: 10.1002/jcp.24486
- Piccin A., Murphy W. G., & Smith O. P. (2007) Circulating microparticles: pathophysiology and clinical implications. *Blood reviews*, 21(3):157–171. doi: 10.1016/j.blre.2006.09.001

- Puhka M., Takatalo M., Nordberg M. E., Valkonen S., Nandania J., Aatonen M., Yliperttula M., Laitinen S., Velagapudi V., Mirtti T., Kallioniemi O., Rannikko A., Siljander P. R., & Af Hällström T. M. (2017) Metabolomic profiling of extracellular vesicles and alternative normalization methods reveal enriched metabolites and strategies to study prostate cancer-related changes. *Theranostics*, 7(16): 3824–3841. doi: 10.7150/thno.19890
- Rana S., Yue S., Stadel D. & Zoller M. (2012) Toward tailored exosomes: the exosomal tetraspanin web contributes to target cell selection. *The international journal of biochemistry & cell biology*, 44: 1574-1584. doi: 10.1016/j.biocel.2012.06.018
- Raposo G. & Stoorvogel, W. (2013) Extracellular vesicles: Exosomes, microvesicles, and friends. *Journal of Cell Biology* 200(4): 373–383. doi: 10.1083/jcb.201211138
- Rodig, S. J. (2019). Detecting horseradish peroxidase-labeled cells. *Cold Spring Harbor Protocols* (4): pdb-prot099713. doi: 10.1101/pdb.prot099713
- Skog J., Würdinger T., van Rijn S., Meijer D.H., Gainche L., Sena-Esteves M., Curry W.T., Jr, Carter, B.S., Krichevsky A.M., & Breakefield X.O. (2008) Glioblastoma microvesicles transport RNA and proteins that promote tumour growth and provide diagnostic biomarkers. *Nature Cell Biology*, 10(12):1470–1476. doi: 10.1038/ncb1800
- Smyth, T., Kullberg, M., Malik, N., Smith-Jones, P., Graner, M.W., & Anchordoquy, T.J. (2015) Biodistribution and delivery efficiency of unmodified tumor-derived exosomes. *Journal of Controlled Release*, 199: 145-155. doi: 10.1016/j.jconrel.2014.12.013
- Takahashi Y., Nishikawa M., Shinotsuka H., Matsui Y., Ohara S., Imai T., & Takakura Y. (2013) Visualization and *in vivo* tracking of the exosomes of murine melanoma B16-BL6 cells in mice after intravenous injection. *Journal of Biotechnology*, 165(2): 77-84. doi: 10.1016/j.jbiotec.2013.03.013
- Thermo Fisher Scientific (2016) Nanodrop 2000/2000c Protein Assay Guide. Technical Bulletin. Retrieved from <https://assets.fishersci.com/TFS-Assets/CAD/manuals/T032-NanoDrop-2000-2000c-Protein-Measurements.pdf>
- Toyofuku M., Nomura N. & Eberl L. (2019) Types and origins of bacterial membrane vesicles. *Nature Reviews Microbiology* 17: 13–24. doi: 10.1038/s41579-018-0112-2
- Tulkens J., De Wever O. & Hendrix A. (2020) Analyzing bacterial extracellular vesicles in human body fluids by orthogonal biophysical separation and biochemical characterization. *Nature Protocols*, 15: 40–67. doi: 10.1038/s41596-019-0236-5
- Van Deun J., Mestdagh P., Sormunen R., Cocquyt V., Vermaelen K., Vandesompele J., Bracke M., De Wever O. & Hendrix A. (2014) The impact of disparate isolation methods for extracellular vesicles on downstream RNA profiling, *Journal of Extracellular Vesicles* 3: 24858. doi: 10.3402/jev.v3.24858
- van Niel G., Raposo G., Candalh C., Boussac M., Hershberg R., Cerf-Bensussan N., & Heyman M. (2001) Intestinal epithelial cells secrete exosome-like vesicles. *Gastroenterology*, 121(2): 337-349. doi: 10.1053/gast.2001.26263
- Wei S., Peng W., Mai Y. Li K., Wei W., Hu L., Zhu S., Zhou H., Jie W., Wei Z., Kang C., Li, R., Liu Z., Zhao B. & Cai Z. (2020) Outer membrane vesicles enhance tau phosphorylation

and contribute to cognitive impairment. *Journal of Cell Physiology*, 235: 4843– 4855. doi: 10.1002/jcp.29362

Wiklander O., Nordin J.Z., O'Loughlin A., Gustafsson Y., Corso G., Mäger I., Vader P., Lee Y., Sork, H., Seow Y.,Heldring N., Alvarez-Erviti L., Smith C., Le Blanc K., Macchiarini P., Jungebluth P., Wood M. & Andaloussi S. (2015) Extracellular vesicle *in vivo* biodistribution is determined by cell source, route of administration and targeting, *Journal of Extracellular Vesicles*, 4:1, doi: 10.3402/jev.v4.26316

Yáñez-Mó M., Siljander P.R., Andreu Z., Zavec A.B., Borràs F.E., Buzas E.I., Buzas K., Casal E., Cappello F., Carvalho J., Colás E.,Cordeiro-da Silva A.,Fais S., Falcon-Perez J.M., Ghobrial I.M., Giebel B., Gimona M., Graner M., Gursel I. ... & De Wever O. (2015) Biological properties of extracellular vesicles and their physiological functions. *Journal of Extracellular Vesicles*, 4: 27066 doi: 10.3402/jev.v4.27066

Yao Z., Qiao Y., Li X., Chen J., Ding J., Bai L., Shen F., Shi B., Liu J., Peng L., Li J., & Yuan Z. (2018) Exosomes exploit the virus entry machinery and pathway to transmit alpha interferon-induced antiviral activity. *Journal of virology*, 92(24): e01578-18. doi: 10.1128/JVI.01578-18

Zhang H. G., & Grizzle W. E. (2011) Exosomes and cancer: a newly described pathway of immune suppression. *Clinical Cancer Research*, 17(5), 959-964. doi: 10.1158/1078-0432.ccr-10-1489

Zhao, H., Yang, L., Baddour, J., Achreja, A., Bernard, V., Moss, T., Marini, J.C., Tudawe T., Seviour E.G., San Lucas F.A., Alvarez H., Gupta, S. Maiti S.N., Cooper L., Peehl D., Ram P.T., Maitra A. & Nagrath, D. (2016) Tumor microenvironment derived exosomes pleiotropically modulate cancer cell metabolism. *eLife* 5: e10250. doi: 10.7554/eLife.10250